AFRL-RD-PS-
TR-2017-0054

# ENERGY STORAGE DEVICES AS PRIME POWER SUPPLIES FOR LOW ENERGY, HIGH VOLTAGE MARX GENERATORS

**David Wetz**

**University of Texas at Arlington**
**416 Yates Street**
**537 Nedderman Hall**
**Arlington, Texas 76019 - 0016**

**30 October 2017**

## Final Report




**AIR FORCE RESEARCH LABORATORY**
**Directed Energy Directorate**
**3550 Aberdeen Ave SE**
**AIR FORCE MATERIEL COMMAND**
**KIRTLAND AIR FORCE BASE, NM 87117-5776**

# NOTICE AND SIGNATURE PAGE

Using Government drawings, specifications, or other data included in this document for any purpose other than Government procurement does not in any way obligate the U.S. Government. The fact that the Government formulated or supplied the drawings, specifications, or other data does not license the holder or any other person or corporation; or convey any rights or permission to manufacture, use, or sell any patented invention that may relate to them.

Qualified requestors may obtain copies of this report from the Defense Technical Information Center (DTIC) (http://www.dtic.mil).

AFRL-RD-PS-TR-2017-0054 HAS BEEN REVIEWED AND IS APPROVED FOR PUBLICATION IN ACCORDANCE WITH ASSIGNED DISTRIBUTION STATEMENT.

HEIDGER.SUSAN.L.1230557760 Digitally signed by HEIDGER.SUSAN.L.1230557760 Date: 2018.03.15 13:57:43 -06'00'

SUSAN HEIDGER, DR-IV
Project Officer

LANGDON.STEPHEN.L.1232187065 Digitally signed by LANGDON.STEPHEN.L.1232187065 Date: 2018.03.15 14:37:06 -06'00'

STEPHEN LANGDON, DR-III
Chief, HPEM Technologies Division

This report is published in the interest of scientific and technical information exchange, and its publication does not constitute the Government's approval or disapproval of its ideas or findings.

# REPORT DOCUMENTATION PAGE

*Form Approved*
*OMB No. 0704-0188*



| **1. REPORT DATE** *(DD-MM-YYYY)* | **2. REPORT TYPE** | **3. DATES COVERED** *(From - To)* |
|---|---|---|
| 30-10-2017 | Final Report | 03-08-2015 – 30-09-2017 |

**4. TITLE AND SUBTITLE**

Energy Storage Devices as Prime Power Supplies for Low Energy, High Voltage Marx Generators

**5a. CONTRACT NUMBER**

**5b. GRANT NUMBER**
FA9451-15-1-0077

**5c. PROGRAM ELEMENT NUMBER**

**6. AUTHOR(S)**

David Wetz

**5d. PROJECT NUMBER**

**5e. TASK NUMBER**

**5f. WORK UNIT NUMBER**
D08E

**7. PERFORMING ORGANIZATION NAME(S) AND ADDRESS(ES)**

University of Texas at Arlington
416 Yates Street
537 Nedderman Hall
Arlington, Texas 76019 - 0016

**8. PERFORMING ORGANIZATION REPORT NUMBER**

**9. SPONSORING / MONITORING AGENCY NAME(S) AND ADDRESS(ES)**

Air Force Research Laboratory
3550 Aberdeen Avenue SE
Kirtland AFB, NM 87117-5776

**10. SPONSOR/MONITOR'S ACRONYM(S)**

AFRL/RDHP

**11. SPONSOR/MONITOR'S REPORT NUMBER(S)**
AFRL-RD-PS-TR-2017-0054

**12. DISTRIBUTION / AVAILABILITY STATEMENT**
Approved for Public Release: Distribution is Unlimited.

**13. SUPPLEMENTARY NOTES**

**14. ABSTRACT**
There is an increasing desire to make pulsed power systems more mobile, compact, and efficient. Pulsed power supplies are used to electrically drive many applications including, but not limited to high power microwave (HPM) sources, electromagnetic launchers, improvised explosive device (IED) defeat systems, lasers, environmental treatment systems, and plasma gas dissolution systems. While many of these loads have only military applications, high voltage pulsed generators have use in driving both military and civilian loads. From a historical perspective, pulsed power research has been performed in large laboratories where size is not typically a limiting factor. Transitioning these large systems into compact devices that can be used by the military in theatre and by everyday civilians is challenging but necessary. Because the emphasis has largely been placed on improving the pulsed power supply, very little research has been performed to reduce the size of the prime power source. While work has been performed on developing mobile prime power supplies that use batteries, it is clear from the documentation that the prime power supply was not given the attention needed optimize their size and efficiency. In this effort, UT Arlington's PPEL has evaluated the fundamental limitations of electrochemical energy storage devices, initially high power lithium-ion batteries and fuel cells, for use as prime power or compact high voltage pulsed power sources.

**15. SUBJECT TERMS**
Prime power, high voltage power sources, batteries, fuel cells, compact power

| **16. SECURITY CLASSIFICATION OF:** | | | **17. LIMITATION OF ABSTRACT** | **18. NUMBER OF PAGES** | **19a. NAME OF RESPONSIBLE PERSON** |
|---|---|---|---|---|---|
| **a. REPORT** | **b. ABSTRACT** | **c. THIS PAGE** | | | Susan Heidger |
| Unclassified | Unclassified | Unclassified | SAR | 54 | **19b. TELEPHONE NUMBER** *(include area code)* |

**Standard Form 298 (Rev. 8-98)**
**Prescribed by ANSI Std. 239.18**

This page intentionally left blank.

## TABLE OF CONTENTS

## LIST OF FIGURES

## LIST OF TABLES

## 1.0 SUMMARY

There is an increasing desire to make pulsed power systems more mobile, compact and efficient than they presently are. Pulsed power supplies are used to electrically drive many applications including, but not limited to, high power microwave (HPM) sources [1-10], electromagnetic launchers [11-14], improvised explosive device (IED) defeat systems [15], lasers [5,6,16-19], environmental treatment systems [20] and plasma gas dissolution systems [21,22]. While many of these loads have only military applications, high voltage pulsed generators several find use in driving both military and civilian loads. From a historical perspective, pulsed power research has been performed in large laboratories where size is not typically a limiting factor. Transitioning these large systems into compact devices that can be used by the military in theatre and by everyday civilians is challenging but necessary [23,24]. Developing compact pulsed power supplies for these various applications has slowly evolved through decades of hard fought research and despite the ability to reduce the volume and mass of nearly all components used in pulsed power sources, the prime power supplies remain relatively large and most often AC grid-tied. This is, of course, a showstopper if these systems are to be usable outside of the laboratory. Because the emphasis has largely been placed on improving the pulsed power supply, very little research has been performed over the years to reduce the size of the prime power source from which the power originates. Many have documented the development of mobile prime power supplies that use batteries but it is clear from the way the work is presented that the prime power supply were not optimized or given the attention needed to make them as compact and efficient as they could have been. With the support of this effort, University of Texas at Arlington's (UTA) Pulsed Power and Energy Laboratory (PPEL) is evaluating the fundamental limitations of electrochemical energy storage devices, initially high power lithium-ion batteries [25-49] and fuel cells [50-52], when they are considered for use as the prime power supply for compact high voltage pulsed power sources.

## 2.0 INTRODUCTION

### 2.1 Lithium-Ion Batteries

Though lithium-ion batteries are still quite technologically immature compared to other electrochemistries, they have advanced considerably over the past two decades, widely opening the application space in which they can be used as either prime or augmenting power. In any application, it is desirable for a battery to store as much energy as possible in the smallest form factor, i.e. have high energy density as shown in Figure 1. Until recently, lithium-ion batteries were available with high energy density but they only possessed a modest power density [53]. This made them the perfect power source for supplying steady energy to a load for a long period but poor for supplying high power to loads that fluctuate or are transient in nature. This was problematic for their deployment in defense applications; especially directed energy systems that demand both high energy and high power from their prime power supply. As they have matured, so has the ability to increase the power density due to dramatic improvements in the electrode structure, internal bus work and electrolyte, which together have increased the double layer capacitance of the cell and reduced the internal impedance. There are several different chemistries of lithium-ion batteries and each of them has its own set of positive and negative characteristics. A few of these characteristic properties include their capacity, operational voltage, power density, energy density, operational temperature range, calendar life, cycle life, cost, maturity and safety.

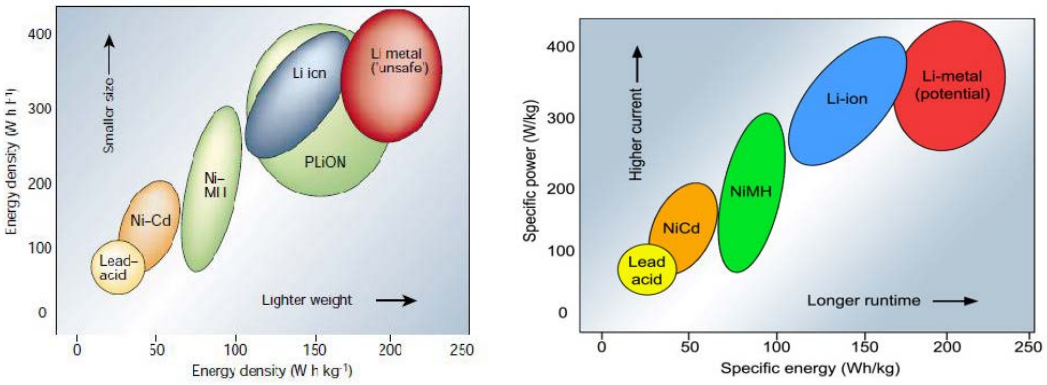


**Figure 1. Ragone Chart Comparing the Volumetric and Gravimetric Energy Densities (left) [54, 55] and Specific Energy and Specific Power (right) Respectively, of Several Different Electrochemical Battery Chemistries**

There are countless research papers published in the open literature documenting the development, fabrication, aging mechanisms, cycle life, safety, etc. of many different types of lithium-ion batteries. A very select few of those are presented in [56-66]. In most of the documented literature, lithium-ion cells are cycled at rates equal to or less than their 1C rating. The 1C rating is the usable capacity that a cell can provide to a load at a current equal to its 1C rating. For example, a 1 Ah cell will supply 1 A to a load for 1 hour. Very few papers are published in which researchers have studied the operation [67-85] and aging of lithium-ion cells at high C rates. There are several reasons for this. First, most research in the area of lithium-ion batteries is focused on understanding the electrochemical kinetics which are best studied at low C rates. Second, the cycle life of a lithium-ion cell is maximized when they are cycled at low rates and at a shallow depth of discharge. Third, the safety of the cells is maximized when they are operated within their rated specifications and given the potential for thermal runaway [86-89], few researchers are willing to risk the safety of the cell. Lastly, it is seldom to none that an engineer will design the battery for a consumer electronics device to operate at rates higher than their 1C rating. This is not the case when engineers are designing a battery prime power source for a directed energy application to be operated aboard a mobile platform. In these applications, it is critical that the battery be designed as small as possible since weight and volume aboard the platform is of incredible value. While many of these applications will require continuous high power to be sourced by the battery supply, most will often only require the battery to supply power in a pulse width modulated manner meaning that operation at rates much higher than 1C is often very feasible. While it has been shown that many commercial off the shelf (COTS) lithium-ion batteries are capable of high continuous and pulsed power operation, virtually no literature exists documenting every type of cell's capability, cycle life, aging mechanisms and safety when they are operated at rates well in excess of their 1C rating. While many manufacturers will publish high rate capacity values and even some discharge curves, little is published much in excess of that. Given this lack of literature, many engineers who design batteries to operate at high rates will overestimate the batteries capacity and voltage at high rates leaving the supply inadequate for the intended application. For these reasons, it is critical that lithium-ion batteries of various chemistries be studied and characterized at high rates under profiles of interest to directed energy applications. In the work discussed here, the PPEL at the UTA has performed research to identify how lithium-ion cells of various chemistries behave and perform, electrically [67-76], chemically [77-81] and thermally [90-94], when they are cycled under high rate profiles of interest to directed energy applications.

## 2.2 Battery Chemistries

There are hosts of metal oxide electrode chemistries that can be used in high power applications. Each of these has their own advantages and disadvantages, which will be discussed, specifically in regards to

temperature stability, energy density and power density. A plot comparing the usable voltage range of a few different chemistries with respect to the active chemistry loading is shown in Figure 2, Figure 3 and Figure 4 respectively. Table 1 lists many of the characteristics used to evaluate lithium-ion batteries and compares them with respect to each other. Though discussion of the chemistry is beyond the scope of this report, there are charge and discharge limitations with each chemistry though by engineering the current distribution tab designs, the electrode coating thicknesses and the electrolyte additives, manufacturers are able to manipulate each chemistries capabilities within reason. In short nearly all chemistries can be engineered for high rate discharge however solid electrolyte interphase (SEI) layer formation in most chemistries other than lithium-titanate oxide (LTO), often limits the recharge to rates less than the discharge limits due to intercalation time required.

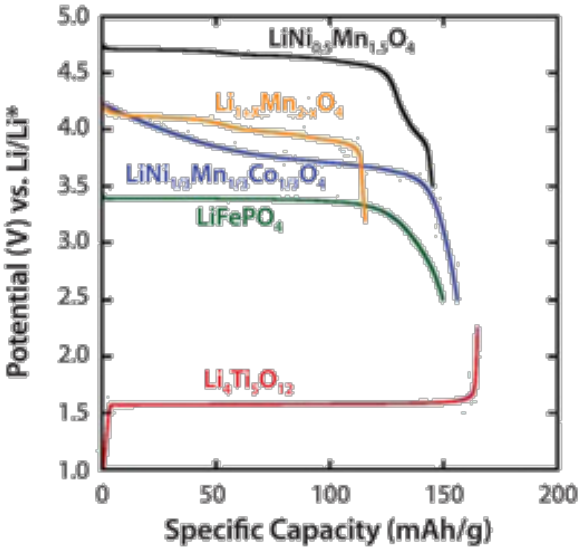


**Figure 2. Plot of Cell Potential vs the Loading of the Active Chemistry used [90]**

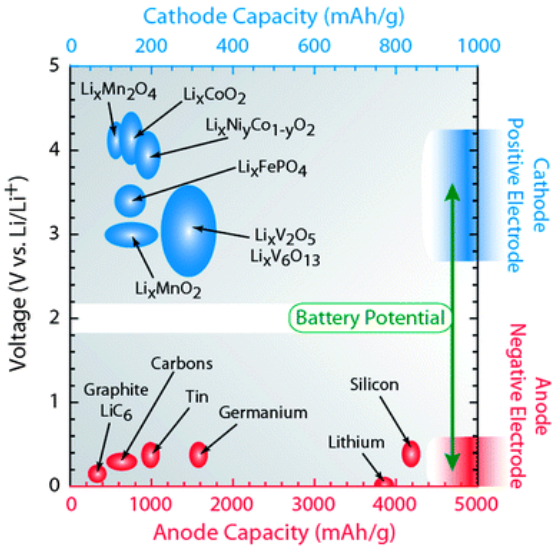


**Figure 3. Capacity and Voltage Comparison Offered by Different Lithium-Ion Battery (LIB) Chemistries Separating out Cathode and Anode Potentials [96]**

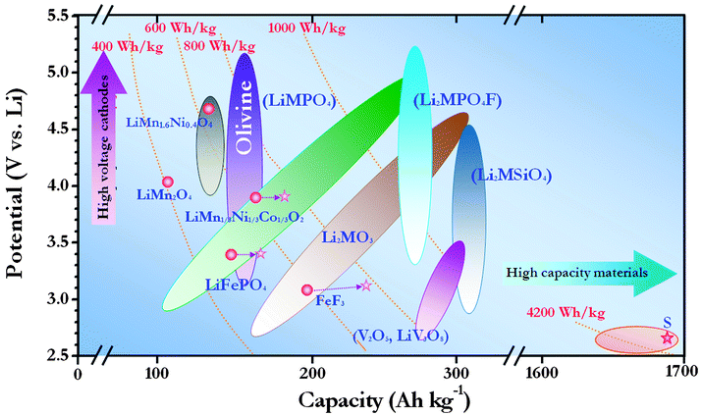


**Figure 4. Capacity and Voltage Comparison Offered by Different LIB Chemistries [96]**

**Table 1. Relative Comparison of the Operational Properties of Lithium-Manganese-Oxide (LMO), Nickel-Cobalt-Aluminum-Oxide (NCA or LiNiCOAlO2), Lithium-Iron-Phosphate (LFP or LiFePO4) and LTO chemistries [97]**

| | LMO | NCA | LFP | LTO |
|---|---|---|---|---|
| Energy | Poor | Good | Average | Poor |
| Power | Good | Good | Good | Good |
| Low Temp. | Good | Good | Average | Good |
| Calendar Life | Poor | Good | Average | Good |
| Cycle Life | Average | Good | Good | High |
| Safety | Average | Poor | Good | High |
| Cost | Average | High | Low | High |
| Maturity | High | High | Medium | Medium |

A common lithium-ion chemistry used in electric vehicles is lithium-nickel-manganese-cobalt-oxide ($LiNiMnCoO_2$). The energy density and power density of this chemistry are hybridized due to the mixing of Ni and Mn. Ni can accommodate higher energy densities while Mn based chemistries have the ability to form a high density spinel structure, see Figure 5, which can reduce the internal resistance of the cell. Varying the ratios of the metals in this chemistry, Ni:Mn:Co, allows for the tailoring of a specific cell to an application which may call for a higher energy or power density respectively.

Another chemistry that is becoming common in high power applications is the olivine structured, see Figure 5, LFP. The specific energy of this chemistry is low compared to that of Co containing electrodes. Due to the stability that this structure provides, this chemistry is considered one of the safest on the market, as it does not enter thermal runaway upon overcharging or overheating. Since LFP alone has a lower conductivity than spinel based oxides, it is often blended with carbon particles to decrease the internal resistance of the cell. The LFP chemistry has a higher rate of self-discharge than other chemistries making them ideal for short high power applications while still having higher energy density than a supercapacitor. The Deltran batteries being studied here are of the LFP chemistry.

Like the nickel-manganese-cobalt (NMC) chemistry discussed previously, the NCA chemistry is able to stabilize the high energy dense Ni based metal oxide electrodes by adding small amounts of Al. The result is a high-energy dense chemistry with moderate power density. The NCA chemistry utilizes a layered cathode architecture like is shown in Figure 5. The safety of this chemistry is not on par with chemistries

such as LFP in that overcharging promotes the onset of thermal runaway. Even with these safety shortcomings, this chemistry was chosen by Elon Musk as the power supply for the Tesla vehicle powertrains. Like NMC, the metal ratios can be altered to tailor the cell to an application. Higher Al doping levels will decrease the capacity of the cell while providing a more stable structure with lower internal resistance for higher rate capability [100]. The Saft SL2A batteries studied here are of the NCA chemistry.

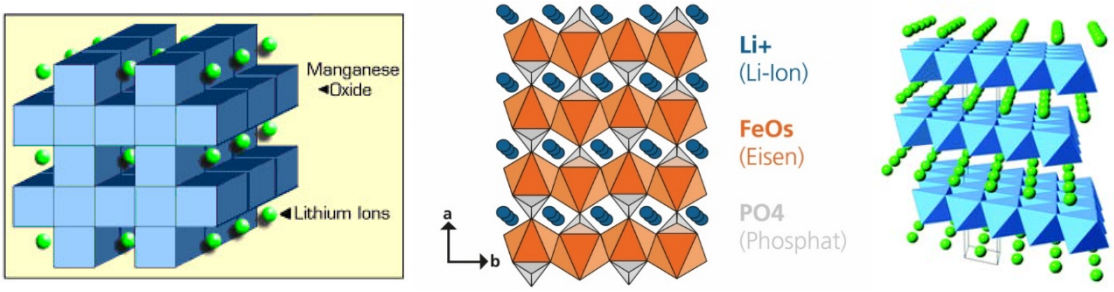


**Figure 5. The Spinel Structure of the NMC Chemistry (left) [98], Olivine Structure of the LFP Chemistry (middle) [99] and Layered Structure of the NCA Chemistry (right) [100]**

On the other hand, LTO cells increase rate capability by replacing the normal graphite anode with lithium titanate, see Figure 6, while the cathode is a graphite with a structure resembling the metal oxides just discussed. Most often, the LTO cells still utilize the same NCA cathode as normal NCA cells. This chemistry has a very low energy density while boasting very high rate capability in comparison to any other battery chemistry discussed here with the exception of LFP. Compared to LFP, LTO cells typically have longer cycle lifetimes and can achieve up to thirty times it nominal capacity rate in pulsed discharge settings. LTO chemistries are also able to be recharged at rates equal to their discharge rate since the SEI interphase layer that limits charge intercalation is removed by the titanate based anode. Also, due to its stability, LTOs have a wide operating temperature range making them one of the safest lithium-ion chemistries on the market. Of all the metal oxide chemistries LTO has the lowest energy density registering around 80 Wh/kg but also boasts the longest life span [98].

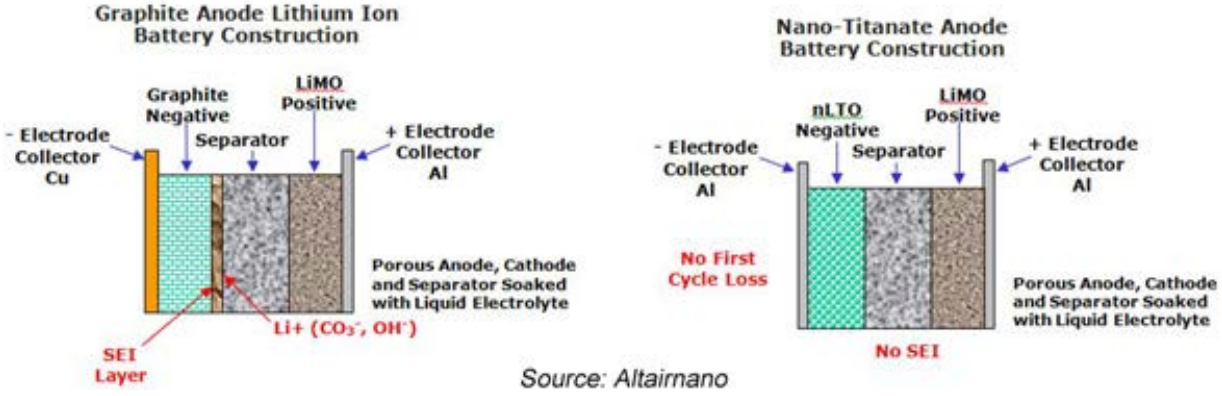


**Figure 6. Graphical Comparison of a Lithium-Metal-Oxide Cathode Battery Utilizing a Graphite (left) and Titanate (right) Based Anode [101]**

Low temperature performance of lithium-ion batteries is mostly determined by the charge transfer resistance, which is strongly influenced by the type of electrolyte mixture used and the choice of conducting salts. Many modern cells use a mixture of organic solvents along with hexafluorophosphate (LiPF6) conducting salt as the mixture to fill the cell and polymer separator. At extremely low temperatures, the

ionic conductivity of the electrolyte is greatly reduced affecting the rate capability and usable capacity. Researchers are still working to fix these issues by formulating new electrolytes with lower freezing temperatures. This excludes the possibility of using LiPO based electrolytes since they usually operate best at or above room temperature. The switch to LiBF4 as the conducting salt in the non-aqueous organic solvent mixture has also improved the low temperature capability of lithium-ion cells. By reducing the resistance at the interface of the electrodes and increasing the rate of low temperature diffusion, cycling lithium-ion batteries below their normal operational temperatures is possible [102-103].

Each chemistry can be designed into 'power' cells or 'energy' cells. Power cells have lower equivalent series resistance (ESR) than energy cells enabling them to supply significant current with less voltage drop across the cell. Typically, the electrodes in power cells are thinner than the electrodes in energy cells, this is to allow intercalation and de-intercalation to occur easier and quicker. Power cells nearly always have a lower energy density than energy cells do, which is a tradeoff that must be considered. The use of hybrid energy storage modules (HESMs) that combine power and energy dense devices are being widely considered as a way to maximize the benefits of both power and energy dense technologies within a single power supply topology [104-112]. Though HESMs are amazing conceptually, implementation is often difficult. In passive designs, care must be taken to ensure the voltage deviation of the more power dense devices is managed when high currents are supplied. To overcome this, active designs are often used that control the power flow from each device so that the voltage requirements are maintained. This requires additional power electronics and control systems, which can increase costs and complexity of the system. Regardless of the disadvantages, HESMs have been demonstrated and proven to maximize the power and energy benefits of different energy storage devices.

## 2.3 Safety

In recent years, several incidents have brought the safety of lithium-ion batteries to the forefront leaving many concerned about the potential dangers they introduce to an electronic system [86-89]. While safety should of course always be a concern, countless systems which utilize very high-energy batteries have been very successfully deployed without incident. Safe operation requires that the batteries be well understood including their aging and failure mechanisms when used at the rates of interest to the application. The use of proper modeling tools, proper thermal management and proper battery management systems (BMS) makes the implementation of a high-energy LIB very safe and feasible. These concerns make the work carried out here even more valuable so that there is an understanding of each cell's high rate operation characteristics.

As one may expect, the lithium-ion chemistries that possess the highest energy density come with the added risk of decreased safety making them attractive but then also unattractive for use in many devices. In many applications in which battery size is not as critical a factor, safer chemistries such as LFP or LTO may be used to decrease the safety risk; however, as expected the battery must be made bigger to store the same amount of usable energy stored in the more dangerous chemistries. The safety concerns in lithium-ion batteries stem from the electrolyte used, which is a solution consisting of organic solvent and inorganic salt [55]. The most common solvents used in lithium-ion batteries are the ethylene carbonate (EC), propylene carbonate (PC), dimethyl carbonate (DMC), diethyl carbonate (DEC) and combinations thereof. LiPF6 is by far the most widely used electrolyte salt in lithium-ion batteries. The thermal stability is poor even at moderately elevated temperatures of 60-85$^{o}$C. It should be mentioned that while many are often scared by the lithium-ion catastrophes that have occurred, it is possible to build high rate batteries using all available chemistries if they are engineered properly. Often times, the catastrophes are a result of improper assembly, a failed BMS, inadequate control, or inadequate cooling schemes. Proper attention to all of these, especially when using the more dangerous, high-energy dense devices, will enable batteries to be safely designed and deployed.

## 2.4 Charging Procedures

When charging a LIB, most often a constant current (CC) – constant voltage (CV) procedure is used. During the CC portion, a continuous DC current is applied to the cell, which is proportional to the cell's C rating, until the cell's maximum manufacturer recommended voltage is reached. Once that voltage is reached, the charging source's voltage is held constant and the charge current is allowed to decay until a pre-determined current threshold is met. Typically, the current limit is set around 0.1C however that varies considerably depending upon the state of charge (SOC) desired and the amount of time that is available for charging. This type of process is shown graphically in Figure 7.

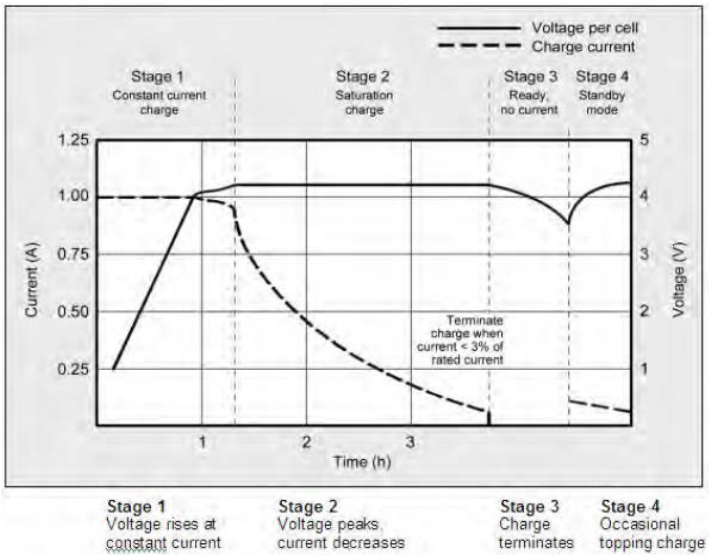


**Figure 7. Plot Graphically Illustrating the CC – CV Charge Procedure of a Rechargeable Battery [113]**

## 2.5 Modeling

In its simplest form, a LIB looks electrically like a large capacitor with an ESR. In reality, there are many different contributors to the ESR as shown in Figure 8. These components include the ohmic resistance of the cell's components, the resistance of the SEI layer formed at the interface of the anode and electrolyte, the electronic resistance associated with de-intercalating a lithium-ion in and out of the electrode structures and the resistance associated with ion diffusion. Each of these terms has its own RC circuit associated with it that contributes to the cell's transient response. Because the storage capacitance and ohmic resistance are the dominating terms, the other contributors are often neglected however, the reader should always be aware of their existence for complete accuracy. The models developed in this work are empirically based models that utilize many elements of the circuit shown in Figure 8. More about that will be discussed later.

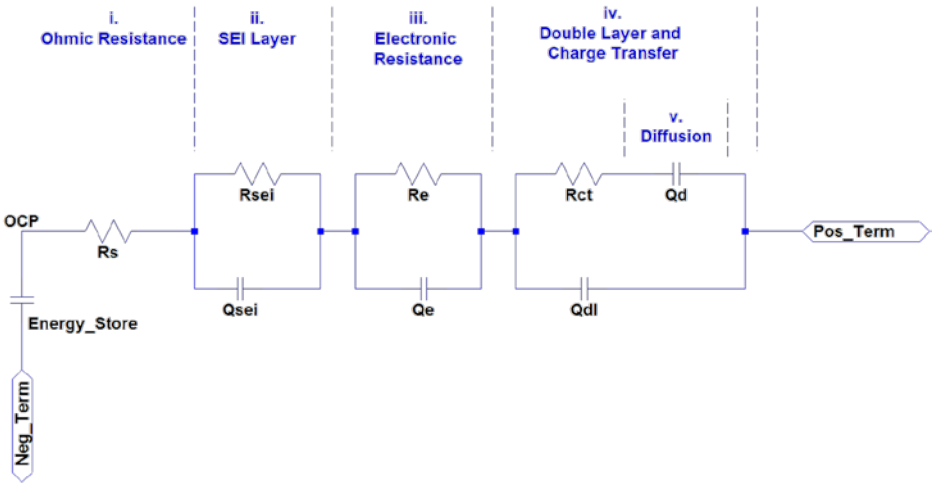


**Figure 8. lithiumalent Circuit Model of a Lithium-Ion Cell [114]**

## 2.6 ESR

Many techniques can be used to measure the impedance of lithium-ion cells. One method involves discharging the cell under test in a short-pulsed manner. By taking the difference in the cell's open circuit potential (OCP) and the conduction voltage early in the pulse and dividing it by the current flow, the resistance can be estimated. This technique is useful if the cell is only going to be used for single short-pulsed discharges but not for much else since a cell's internal impedance varies considerably with temperature, as will be shown later. When longer-term pulsed or continuous discharge is required for an application, it is better to use the average voltage across a wide SOC window to make the DC impedance measurement. The SOC window over which the voltage is averaged should range from somewhere between 10% and 90% in order to avoid the strong voltage inflections present between 0% and 10% and 90% and 100% SOC respectively. By taking the average conduction voltage between 10% and 90% at the high rate of interest and subtracting it from the average conduction voltage at low rates, typically less than ½C and dividing that value by the difference in conduction current, the average DC impedance of the cell can be obtained. As mentioned previously, the impedance varies as a function of temperature so this will only provide an average impedance, not impedance as a function of SOC however, the latter type of measurement can also be obtained through careful manipulation of the data. By using a low rate discharge as the voltage from which the high rate discharge is subtracted, it is assumed that the temperature at low rate does not rise and play a role leaving the temperature at the higher rate discharge to play the dominant role. Figure 9 plots the conduction voltages for a random lithium-ion cell and a simple relationship of how its impedance varies as a function of temperature and SOC.

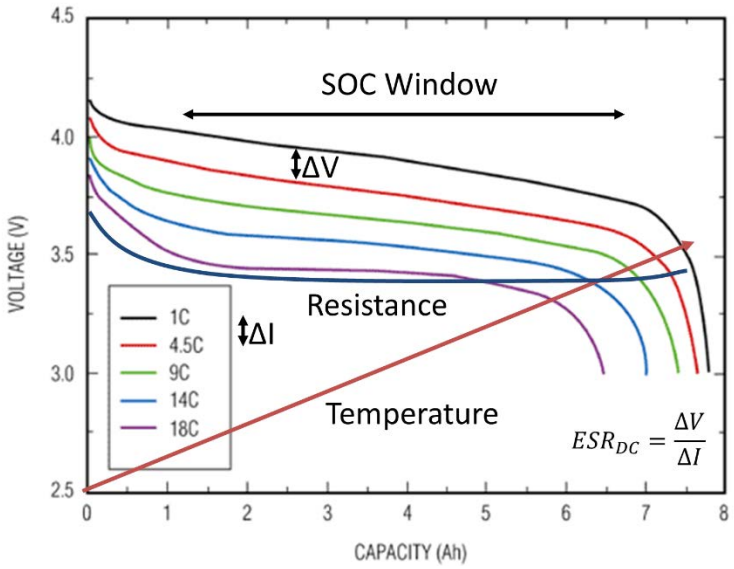


**Figure 9. Graphical Representation of the DC Impedance of a Lithium-Ion Cell. Temperature Arrow is used to Indicate that these Trends are Representative of what Happens as Temperature goes Up**

## 2.7 Electrochemical Impedance Spectroscopy (EIS)

Finally, in order to measure the frequency dependent impedance spectra of a lithium-ion cell, a measurement known as EIS is used. To make an EIS measurement, a device called a potentiostat is used to apply a small sinusoidal perturbation, over a range of frequencies, typically 20 kHz to 10 mHz, across the cell's OCP. Through precise knowledge of the sinusoidal voltage amplitude and measurement of the resulting current, the real and imaginary impedance of the cell across the frequencies applied can be calculated. As just defined, this is a potentiostatic EIS measurement. A similar method applying a known current and measuring the voltage can also be performed. This is called a galvanostatic measurement. Regardless of which measurement technique is used, the resulting impedance spectra can be used to characterize the cell's impedance across frequencies and variation in the impedance can be used to understand how the cell is aging as a function of cycle life. As show in Figure 10, the EIS nyquist plot can be used to identify changes to the various contributors of impedance shown earlier in Figure 8. By making EIS measurements periodically throughout a cell's lifetime, changes in the nyquist plot can be used to identify what portions of the cell are aging. An example of this is shown in Figure 11, where cycle life experiments made on a K2 Energy 26650P cell reveal that the ohmic resistance, shift in the curves to the right and the charge transfer resistance, increase in the first hump's radius, greatly increase throughout its cycle life when cycled 10C discharge and 3C recharge rates [76]. What these impedance shifts imply is that it is getting harder for ions to migrate in and out of the anode electrode. Previous results at UTA on NCA cells has revealed that at high rates, the electrodes heat up and feel strong electromagnetic stress that causes them to crack. This results in a decreased usable capacity and increased overall resistance [75]. These results are similar to those previously published by [82]. In similar work with LFP cells, it has been found that the usable lithium of LFP cells is not depleted when they are cycled at high-pulsed rates. Instead, the interphase resistance layers are increased, further increasing the difficulty ions face migrating in and out of the electrode structures [80]. In the work performed here, significant cycle life is not being studied; however, EIS is being used to provide a baseline impedance measurement of the cells of interest.

As mentioned, it has been shown by UTA and others that at high rates, electrode cracking is limitation contributing to aging. Under low rate operation, the loss of active lithium, growth of the SEI layer and electrolyte decomposition all primarily contribute to cell aging. Aging of energy cells and power cells should not be too much different if they are run under their own recommended specifications. Energy cells

typically have a higher ESR so attempts to operate them at high rate will result in higher heat generation rates and therefore faster aging. Since power cells have thinner electrodes, their structure is a bit weaker allowing them to crack easier under high electrical and mechanical stresses.

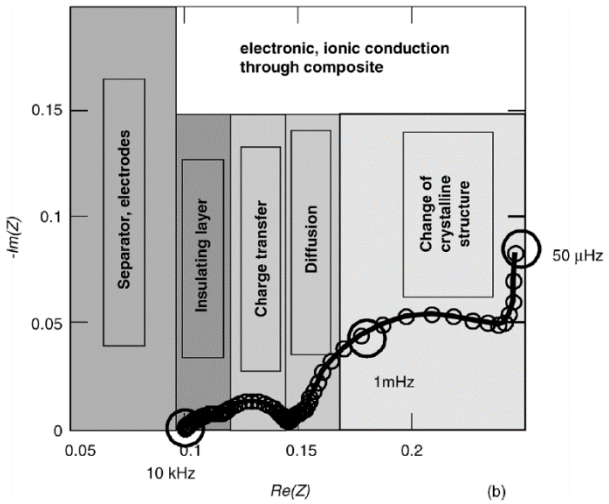


**Figure 10. Graphical Representation of an EIS Nyquist Plot and its Relationship to the Various Contributors of Impedance within a LIB [114]**

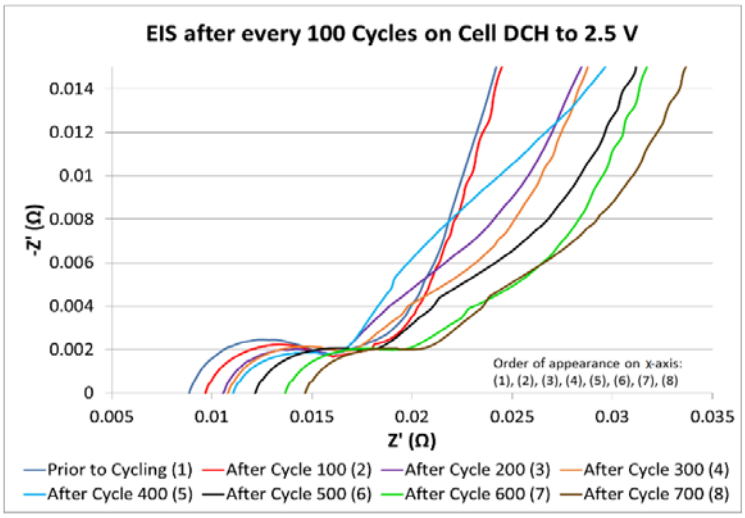


**Figure 11. EIS Measurements Made from a K2 26650P Cell when Discharged to 2.5V at 10 C and Recharged at 3C. A Sinusoidal Perturbation of 10 mV is Applied Across a Frequency Range of 10 kHz to 10 mHz [76]**

## 2.8 Aging Mechanisms

Though the focus of this work is not to study the aging of lithium-ion cells, a small amount of background will be provided. The nature of the LIB creates a complex and intertwined aging process that poses a challenge to properly understanding the process. It is generally understood that calendar or cyclic aging can lead to or can be caused by changes of the electrode/at the electrolyte interface and in the electrolyte, changes of the active material, or changes of the composite electrode (current collector, active materials, conductive additives, binder, porosity, etc.) [77-79]. Cathode materials can have a significant

effect on the performance and aging of lithium-ion cells in both calendar and cycling conditions. Figure 12 illustrates a basic overview of the dominant aging features including changes occurring with the inactive components (binder, current collector, etc.), as wells as the lithium metal oxide. These effects are heavily dependent on the design and production of the cathode material and are truly intertwined making it difficult to examine each independent of the other. Generally, these mechanisms can be grouped into three categories, structural changes during cycling, chemical decomposition/dissolution reaction, or surface film modification. These degradation categories are heavily dependent on SOC, cycling conditions and temperature of the cell. Additionally, the intercalation/deintercalation process induces a mechanical strain on the oxide particles as the volume of the material changes. This strain can cause the micro-cracking, loss of contact and continued surface layer formation.

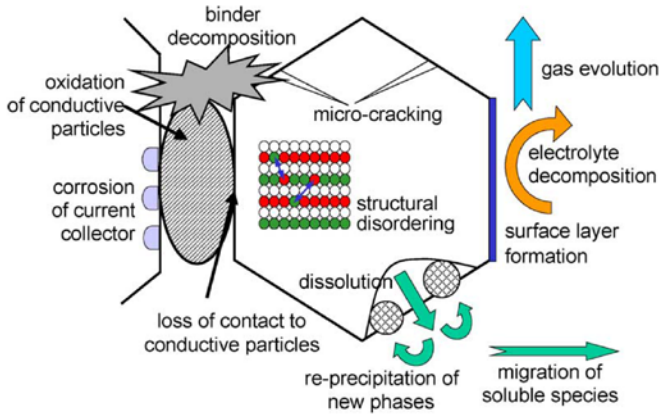


**Figure 12. Overview on Basic Aging Mechanisms of Cathode Materials [56]**

While there has been much research focused on LIB aging, the majority has focused on the changes that occur at the electrode/electrolyte interface because it is considered the primary source for aging at the anode [19-29]. Figure 13 illustrates the primary interactions that take place at the interface including graphite exfoliation and cracking, electrolyte decomposition and SEI formation, SEI conversion, SEI dissolution and lithium plating and corrosion.

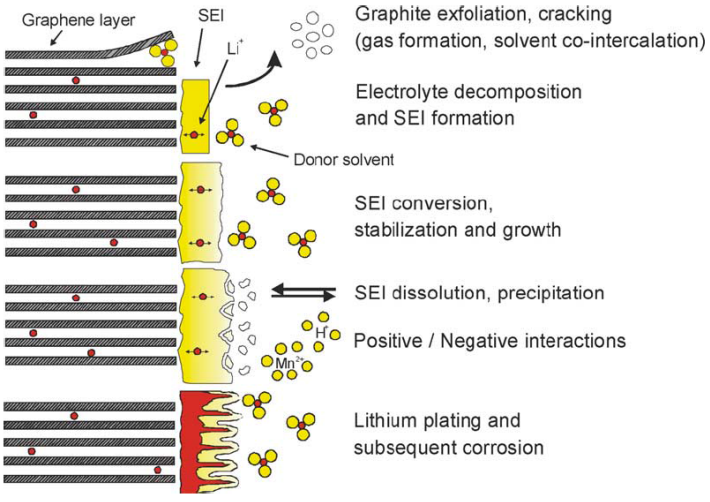


**Figure 13. Changes at the Anode/Electrolyte Interface [56]**

It is well understood that the anode operates at voltages outside of the electrochemical stability of the electrolyte resulting in an irreversible reductive decomposition of the electrolyte at the interface. This reaction results in a buildup of decomposed electrolyte on the surface of the anode that is known as the SEI layer. This buildup typically takes place when the cell is first cycled and prevents continued reduction of the electrolyte. While the SEI allows the intercalation/deintercalation of lithium-ions to and from the anode, it slows the transport increasing the cells total resistance.

## 2.9 Thermal Runaway

Most portable electronic devices today use Lithium Cobalt Oxide (LCO) as their primary cathodic chemistry. While this chemistry can provide the maximum energy density, it is susceptible to thermal runaway when overheated from overcharging or when it is placed in high temperature environments. Overcharging is not of much concern here, because batteries being shipped will generally never be in a charging state. When inactive, high and low temperatures can cause several phenomena within the battery that will cause it to erupt. Low temperature storage and charging can lead to the formation of dendrites that protrude from the surface of the anode [63]. If the dendrites are able to grow large enough and pierce the separator, as seen in Figure 14, it can create an internal short circuit causing the battery to generate a large uncontrollable amount of heat. The heat creates a sharp pressure rise inside the cell due to evaporation of the electrolyte, eventually causing cell eruption once the safety pressure cap bursts. Internal shorts, which can occur from cell manufacturing error or the introduction of impurities, will also usually lead to the generation of an electrical spark that will ignite the flammable electrolyte. A separate problem arises from the degradation of the cathode as the temperature within the cell increases. At high temperatures, the breakdown of LCO liberates oxygen ions that in turn react with the electrolyte to produce gaseous products. This reaction is extremely exothermic and can cause the electrolyte to ignite and burn. As these failure mechanisms are activated, the heat spreads to adjacent cells creating similar effects leading to a cascading failure or domino effect.

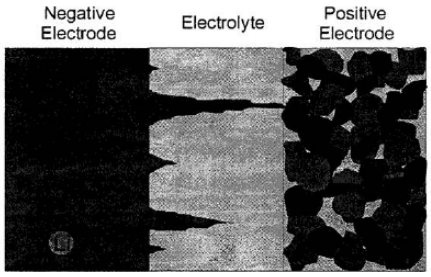


**Figure 14. Dendrite Growth in LIB Can Lead to an Internal Short Circuit and Generation of Heat [63]**

As indicated earlier, safer chemistries such as LFP and LTO have been previously demonstrated at both high energy and high power. Despite making the battery slightly bigger, the safety is often worth it. The US Navy has invested considerable effort into evaluating LFP cells for use in the prime power supply of its electromagnetic railgun (EMRG) [116]. In cases where lithium-ion batteries are simply not suitable, alternative chemistries such as lead acid and nickel metal hydride cells are feasible but these incredibly safe options come with a much greater hit to the energy density and therefore the size of the battery.

In summary, lithium-ion batteries present many opportunities but also many challenges that must be properly considered when operating them at high rate. The above concepts are all important and should be considered when sizing batteries for grid, vehicle and pulsed power applications. Though high-energy chemistries are dangerous, safe batteries can be designed using them if the control, battery management and cooling requirements are met. Batteries benefit from being operated at hotter temperatures, 25°C to 45°C but being stored at lower temperatures. At very low temperatures, intercalation of ions into the graphite is difficult allowing dendrites to grow which can eventually penetrate the separator and internally

short the cell. Finally, when evaluating how lithium-ion cells age, many factors lead to gradual degradation of their usable capacity. In most cases, growth of the SEI layer on the anode leads to capacity fade though in high power applications; it has been shown that cracking of the anode can lead to rapid capacity fade without losing active lithium.

## 3.0 METHODS, ASSUMPTIONS, AND PROCEDURES – LITHIUM-ION BATTERIES

### 3.1 Lithium-Ion Battery Studies for AFRL in FY16/FY17

In this effort, it was proposed that UTA would evaluate, experimentally validate and develop a SPICE model of a Deltran COTS LIB, a Saft SL2A pouch battery and experimentally evaluate the performance of a 20 kW Ballard proton-exchange membrane PEM fuel cell under load profiles, which are representative of how they may be used in peak shaving applications in the electric grid, as high power sources in electric vehicles and finally to drive AFRL compact pulsed power systems. The accomplishments of each task are discussed below.

Several experiments were performed at UTA using programmable loads to experimentally obtain data from the batteries under pulsed discharge rates of interest to AFRL. A photograph of the programmable load, programmable power supply and thermal data logger used in the experiments performed here are shown in Figure 15.

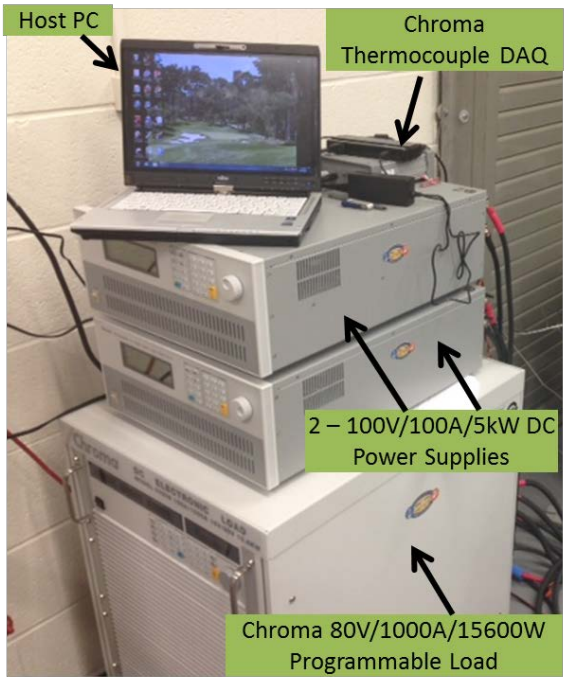


**Figure 15. Photograph of the Programmable Load, Power Supply and Thermal Data Acquisition used to Evaluate the Cells and Modules of Interest here**

The Chroma 63209 programmable load is capable of operating at voltages as high as 80 V, currents as high as 1000 A, or dissipating 15.6 kW of power. Chroma 62050P-100-100 power supplies were utilized to recharge the module after each discharge. The power supplies are each capable of operating at 100 V, supplying 100 A and are limited to 5 kW. High rate recharge is not an element of this study so each recharge is limited to 1C using a CC –CV procedure. A Chroma 51101 thermal data logger was utilized to measure the thermal rise in various places within the module. The thermal logger is able to make eight multiplexed thermal measurements and type T thermocouples were utilized with an accuracy of roughly 1°C. All of the thermocouples were epoxied to the surface they were measuring using thermally conductive epoxy. The

programmable load, programmable power supply and thermal acquisition were all controlled and monitored using a custom written National Instruments (NI) LabVIEW visual instrument (VI) panel running on a host PC that communicates via the GPIB communication protocol.

## 4.0 RESULTS AND DISCUSSION – BATTERY CYCLING

### 4.1 Deltran Results

AFRL expressed interest in studying the performance capabilities of a LFP battery manufactured by Deltran. The battery is of the same form factor as many drop in lead acid batteries, similar to the ones used in many off the shelf uninterruptable power supplies. The size, weight and lifetime of most lead acid UPS batteries are very poor prompting many LIB manufacturers to make lithium-ion versions that are direct replacements for them. AFRL provided UTA with three of the 480 CCA Deltran batteries shown in Figure 16. Also shown in Figure 16 are some usage specifications from the manufacturer's datasheet which are very vague concerning electrical characteristics. The lack of information in any sort of datasheet stems from the types of applications the manufacturer expects these batteries to be used for. Most users will put them into the UPS systems which draw very low rate power from them. In other applications, such grids, vehicles and pulsed power applications, there is a strong need to be able to also draw high peak power from the batteries in the form of short pulses. In grid applications, the burst of power may be needed to meet peak shaving demands that occur on hot days when everyone rushes home to turn on their air conditioning. In, vehicles, there may be a sudden inrush of power required to accelerate the vehicle or alternatively an inrush may need to be absorbed by the battery from sudden regenerative braking systems. In pulsed power applications, the desire is to supply power from the prime power to some form of intermediate energy storage in repetitive manner. For example if a system has a desired rep-rate of ten shots per minute, that means that each shot only has 6 seconds in which the transfer of power from the prime power to the intermediate power as well as the shot must occur. That means that a substantial amount of charge needs to be transferred quickly, requiring the battery to operate at high power. These unique applications are achievable from the battery but the capabilities are not readily available from the datasheet making the work being performed here necessary in order to ensure safe and reliable operation.

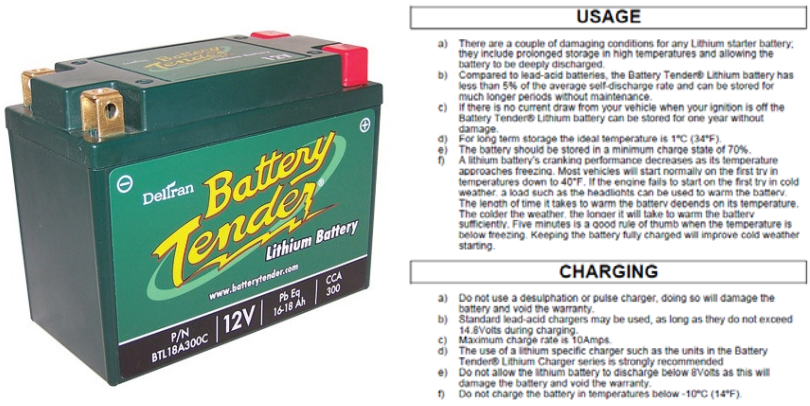


**Figure 16. Deltran Battery Tender LIB (left) and Datasheet Properties (right) [117]**

The first experiments with the module were continuous discharges ranging from 1/2C to 30C. In case the reader is unaware, the C rate is defined by the amount of capacity a battery can supply to a load for 1 hour. If the battery can supply 1 A for 1 hour, it is a 1 Ah battery and has a 1C rate of 1 A. A 30 C rate would be a 30 A discharge and the cell would be able to supply this current for roughly 1/30 of an hour. Figure 17 plots all of the data collected from the 1/2C, 1C, 5C, 10C, 15C, 20C, 25C and 30C rates. As shown, the usable capacity remains quite consistent across these rates. This is typical from lithium-ion

batteries however this battery appears to perform exceptionally well across these rates. The decreasing conduction voltage across rates results from the internal impedance within each cell of the module. As current increases, the voltage drop internal to the cells increases causing the conduction voltage to decrease. This is something that has to be considered when sizing the power electronic converters that condition the power between the prime power and intermediate energy storage devices. Note in the 30C discharge that the curve ends abruptly at roughly 6.4 Ah. That stop was caused by the solder melting that holds the batteries positive terminal onto the output cable. This is not unexpected since these batteries are largely designed for single cold cranking amp event, not continuous discharges at high rates. Because the minimum and maximum rates evaluated are so vastly different, the total time over which each discharge occurs is similarly different. For clarity, the thermal measurements collected from each of the curves in Figure 17 are plotted individually in Figure 18.

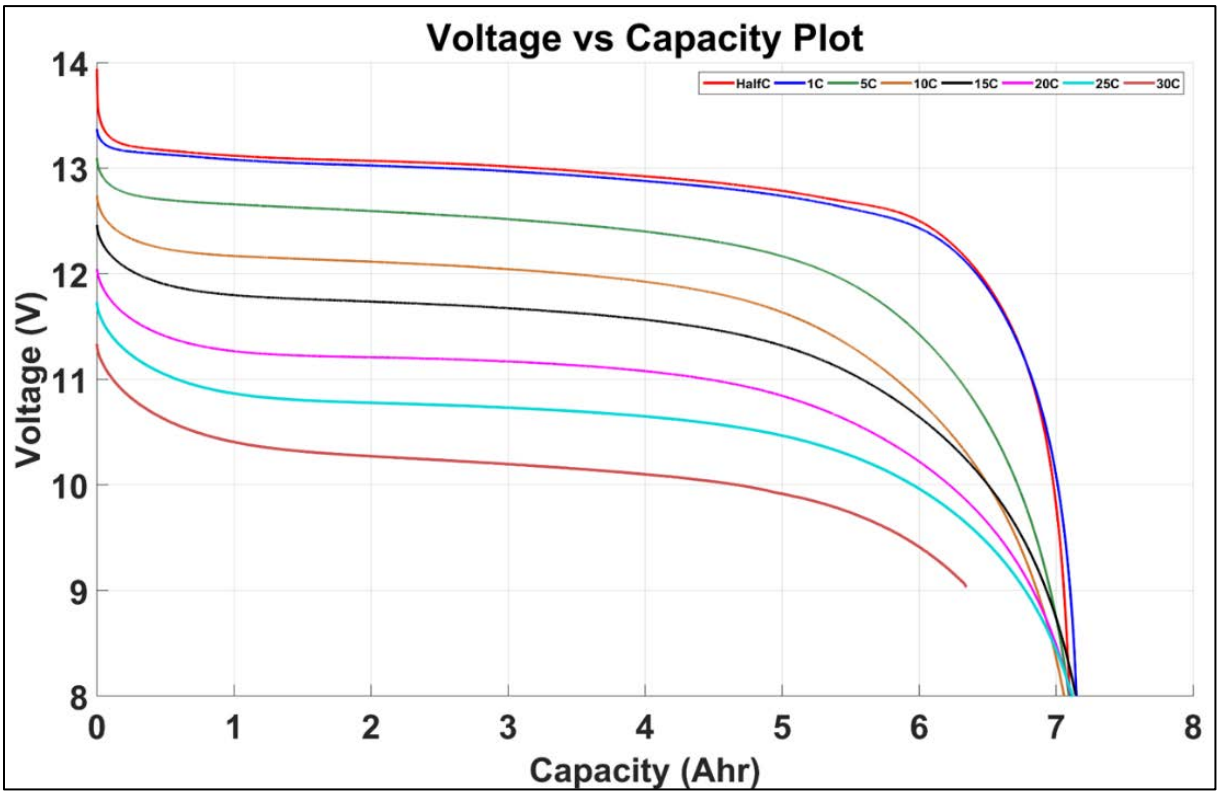


**Figure 17. Deltran Continuous Discharge Voltage at Multiple Rates**

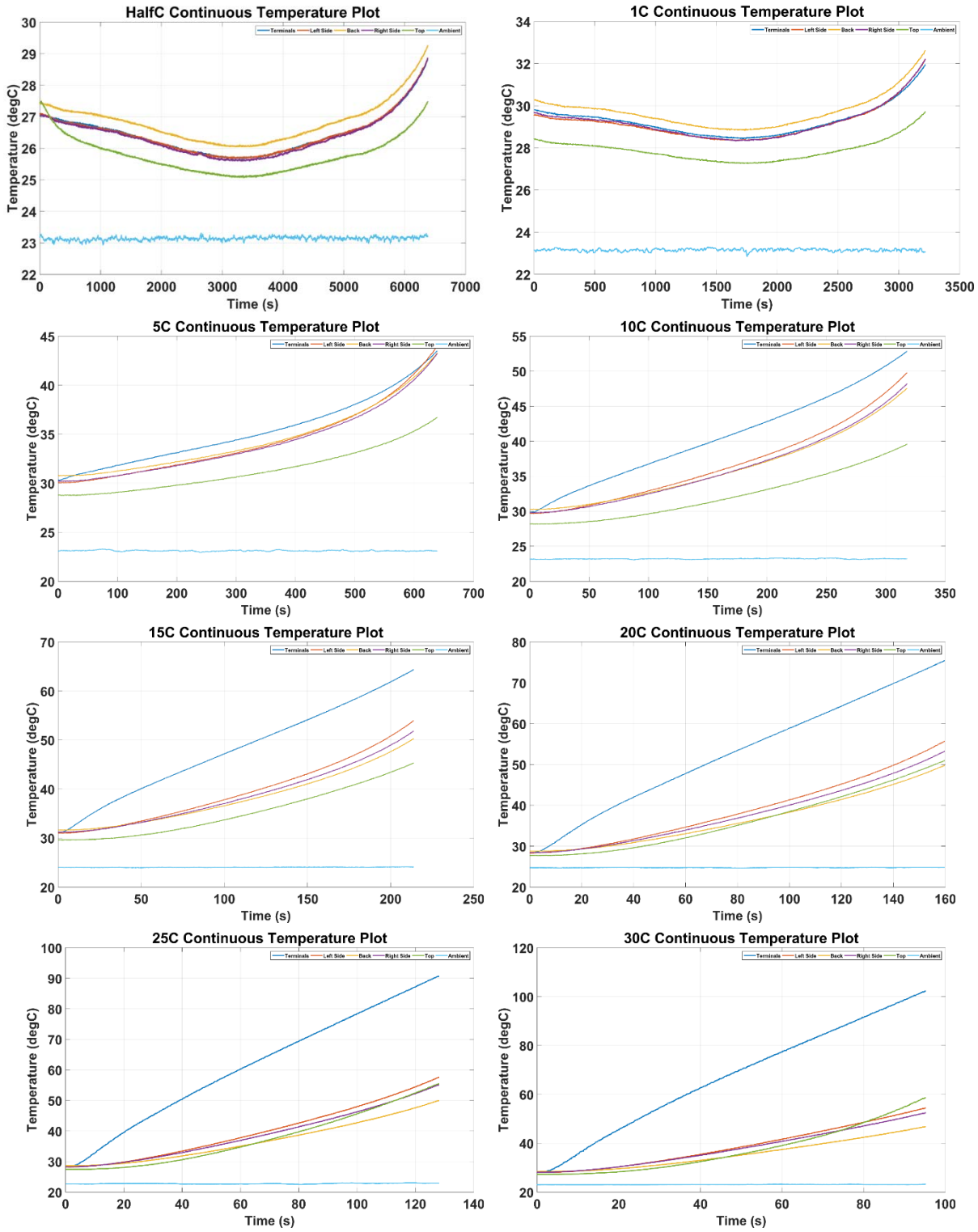


**Figure 18. Deltran 30C Continuous Discharge Temperatures**

The second series of experiments performed involves evaluating the Deltran's performance when they are discharged in a pulsed mode of operation. AFRL expressed interest in a profile that would discharge the module under CC of 900 A for 1 second and then allow it to rest for 59 seconds. The conduction voltage plot is shown in Figure 19 along with the temperature measured. Figure 20 plots similar data collected with

the discharge time is reduced to 0.5 s and the rest time is increased to 59.5 s. Figure 21 plots profiles measured during a 1 s discharge followed by a 59 s rest that is repeated ten times. Note in the temperature profile how there is a ratcheting affect that occurs with each subsequent pulse. Figure 22 plots data collected from ten pulses collected using the 1 s – 59 s profile at a discharge rate of 750 A.

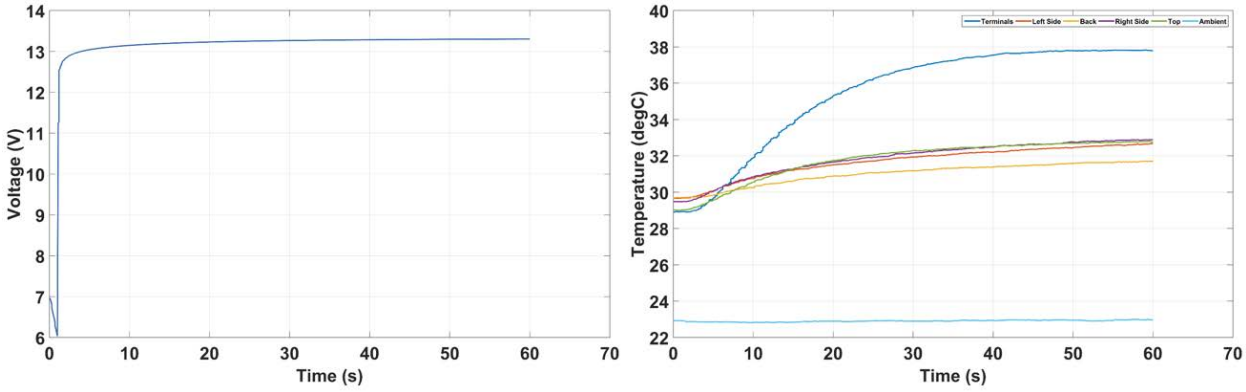


**Figure 19. Deltran Battery Voltage (left) and Temperature (right) During an Ultra-High 1 s – 59 s Current Pulse at a CC of 900A**

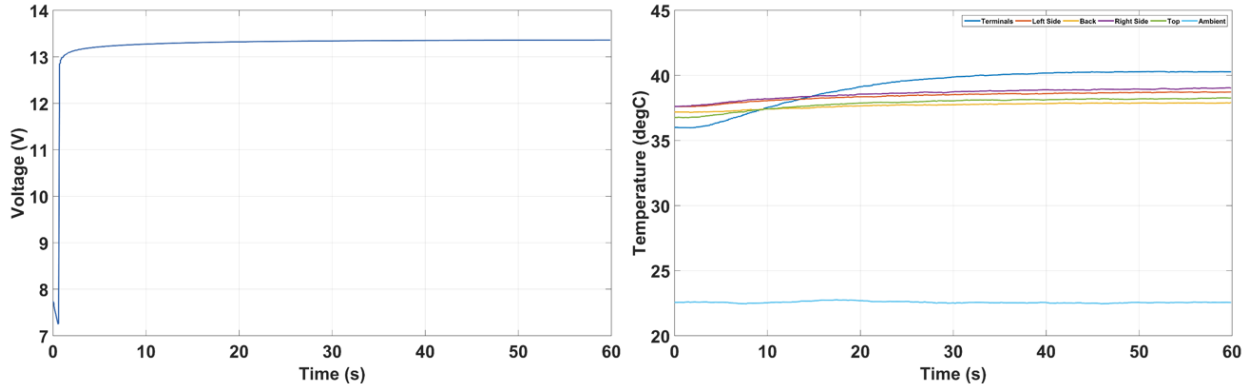


**Figure 20. Deltran Battery Voltage (left) and Temperature (right) During an Ultra-High 0.5 s - 59.5 s Current Pulse at a CC of 900A**

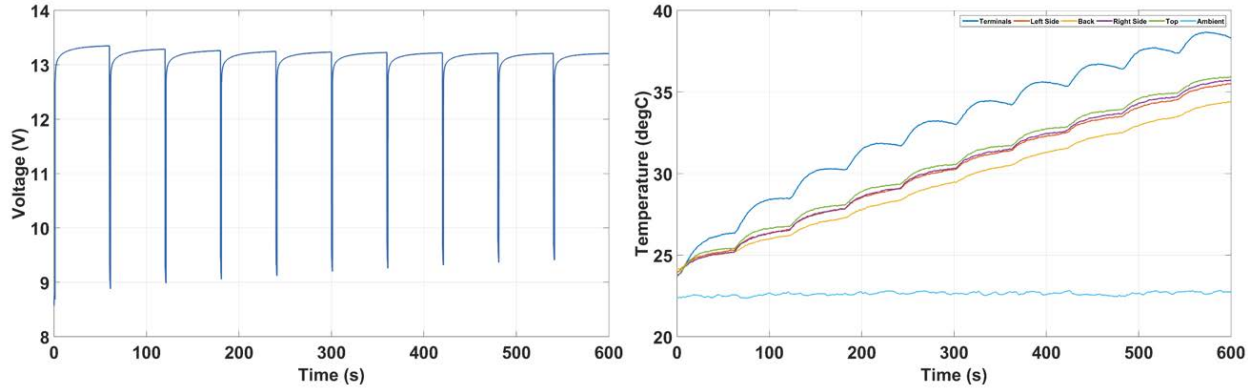


**Figure 21. Deltran Battery Voltage (left) and Temperature (right) During a Repetitive (ten time) Ultra-High 1 s - 59 s Current Pulse at a CC of 500A**

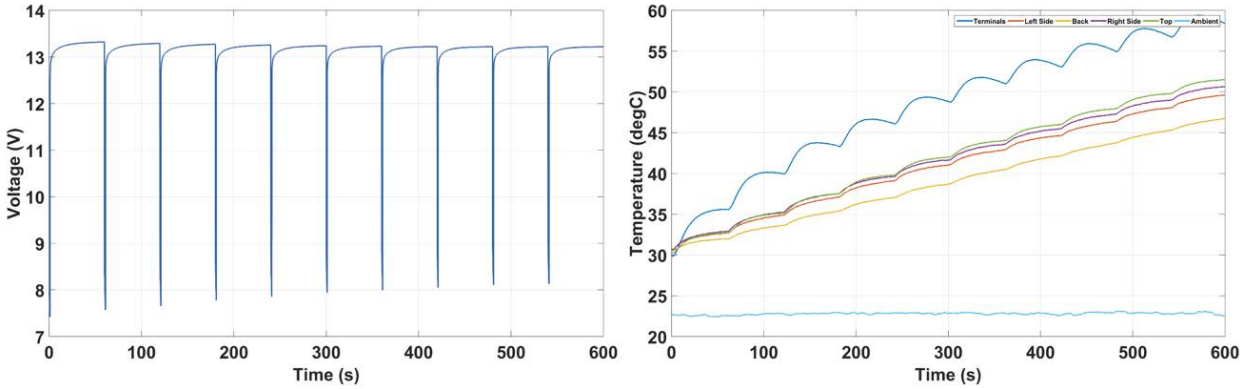


**Figure 22. Deltran Battery Voltage (left) and Temperature (right) During a Repetitive (ten time) Ultra-High 1 s - 59 s Current Pulse at a CC of 750A**

The data presented above demonstrates that the Deltran battery is capable of supplying power at C rates in excess of 100C (900 A / 8 Ah) in a pulsed manner repetitively. The final series of experiments performed were aimed at studying whether or not the module could sustain pulsed discharges throughout its usable capacity. Plots shown in Figures 23 and 24 were obtained when the battery was discharged repetitively at 500 A and 750 A respectively in a 1 s – 59 s pulsed profile until a lower voltage threshold was met. In the case of the 500 A discharge, the lower voltage threshold was 8V while in the 750 A experiment the lower threshold was 6.3 V. The cutoff threshold can be lowered as the current is increased since the voltage is artificially lower due to higher voltage drops at higher current.

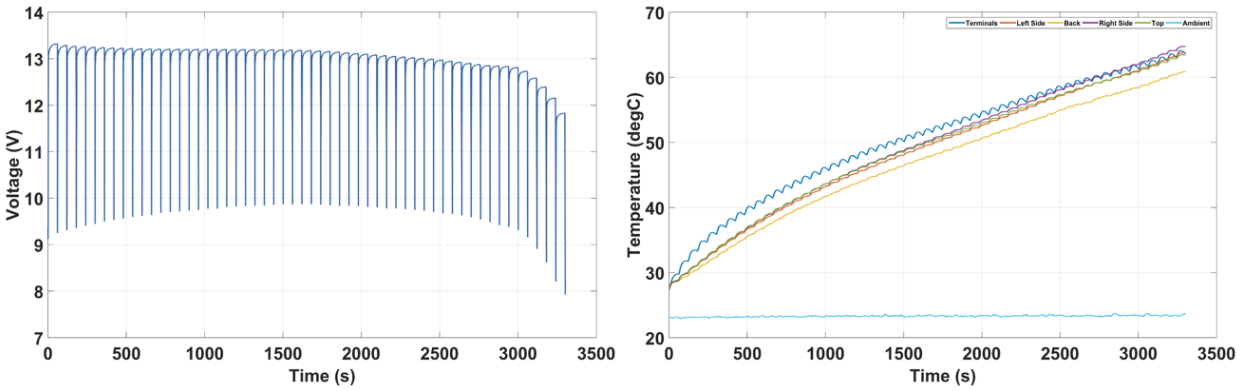


**Figure 23. Deltran Battery Voltage (left) and Temperature (right) During a Repetitive Ultra-High 1 s - 59 s Current Pulse at a CC of 500 A till a Lower Voltage of 8.0 V was Reached**

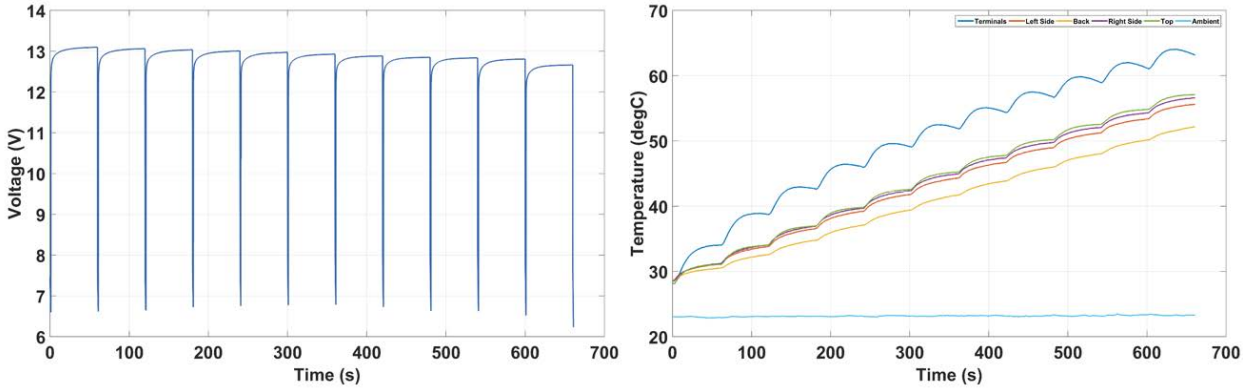


**Figure 24. Deltran Battery Voltage (left) and Temperature (right) During a Repetitive Ultra-High 1 s - 59 s Current Pulse at a CC of 750 A till a Lower Voltage of 6.3 V was Reached**

In summary, the Deltran LIB performed remarkably well given what it is designed for. The battery is capable of supplying very high peak power to repetitively pulsed loads and should be explored further for use in pulsed power applications.

## 4.2 Saft SL2A Results

Unlike the Deltran module, the Saft SL2A NCA pouch cell is better documented and designed for high pulse applications. A photograph is shown in Figure 25 along with manufacturer datasheet properties.

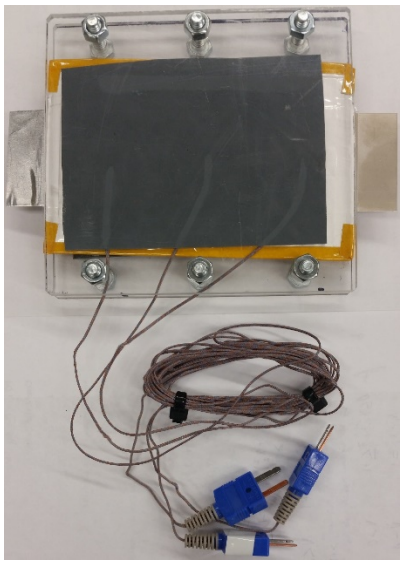

| Electrical characteristics @ 60°C | |
|---|---|
| Rated capacity at C/5[1] (Nominal) | 2.25 Ah |
| Minimum capacity at C/5 | 1.92 Ah |
| Nominal voltage | 3.7 V |
| Nominal energy | 8.3 Wh |
| Recommended maximum discharge current at 65°C | |
| Continuous | 350 A |
| Pulse (2 second) | 400 A |
| Typical power from 100% SOC at 65° C | |
| Continuous (with 400 A as the limit) | 1150 W |
| Pulse (2 second) | 1400 W |
| Maximum impedance at 80°C & 80% SOC at 200A and 2 seconds | 1.85 mΩ |
| Typical impedance at 80°C & 80% SOC at 200A and 2 seconds | 1.65 mΩ |
| **Physical characteristics** | |
| Width[2] | 142 mm |
| Length[3] | 88 mm |
| Thickness | 4.5 mm |
| Mass | 85 g |
| **Cell operating conditions** | |
| Typical cut-off voltage | 2.7 V |
| Charging method | Constant current / Constant voltage |
| Charging voltage | 4.2 V (±0.04 V) |
| Continuous charge current at 25°C | 5C Amps |
| Maxium pulse charge current for 1 second at 80°C | 216 A |
| Maximum charge pulse voltage | 4.3 V |
| Operating temperatures[4] | -30°C to +80°C |
| Storage and transportation temperatures | |
| Recommended | +10°C to +30°C |
| Allowable[5] | -40°C to 70°C |

**Figure 25. Saft SL2A Pouch Cell Photograph (left) and Datasheet Properties (right) [118]**

Several different experiments were performed using the single cell, presented below in Figures 26 through 32. They include continuous discharges from 1/2C to 155 C (Figure 26) and discharges at the same rates under a 5 s discharge/ 1 s rest profile (Figure 27), a 5 s discharge / 5 s rest profile (Figure 28) and a 30 s discharge / 5 s rest profile (Figure 29), respectively. Experiments were also performed in which a single 1 second discharge at a CC of 225 A (Figure 30) was supplied, ten pulses were sourced in a 1 s discharge / 59 s rest profile at a CC of 225 A (Figure 31) and finally full capacity discharges using a 1 s discharge / 59 s rest profile until the cell voltage reached 2.0 V (Figure 32).

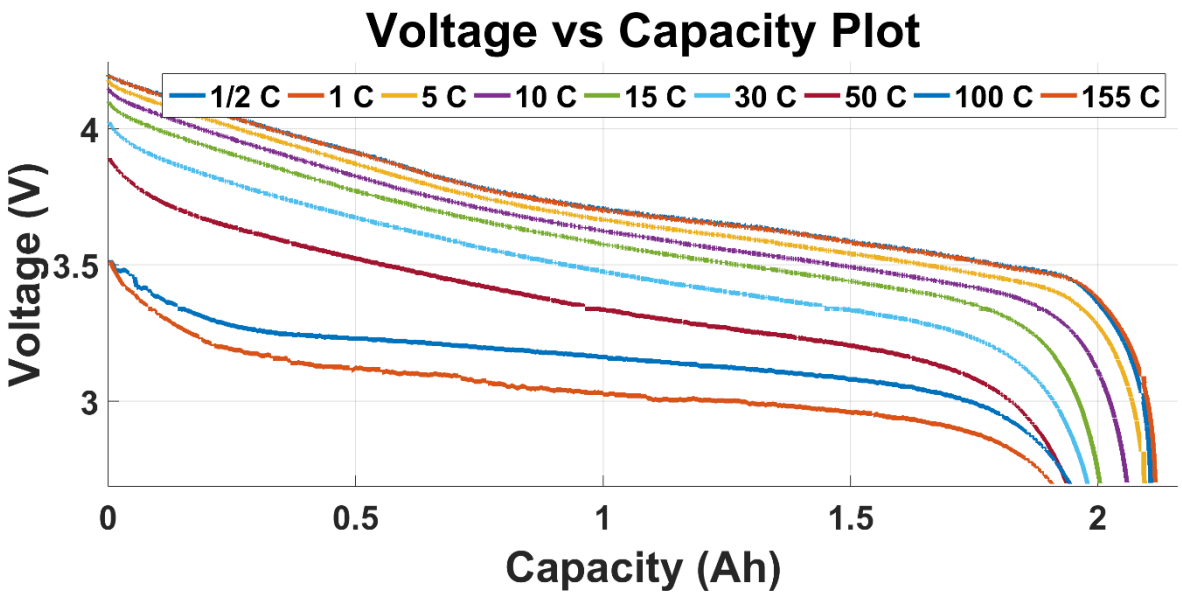


**Figure 26. SL2A Continuous Discharge Voltage vs Capacity**

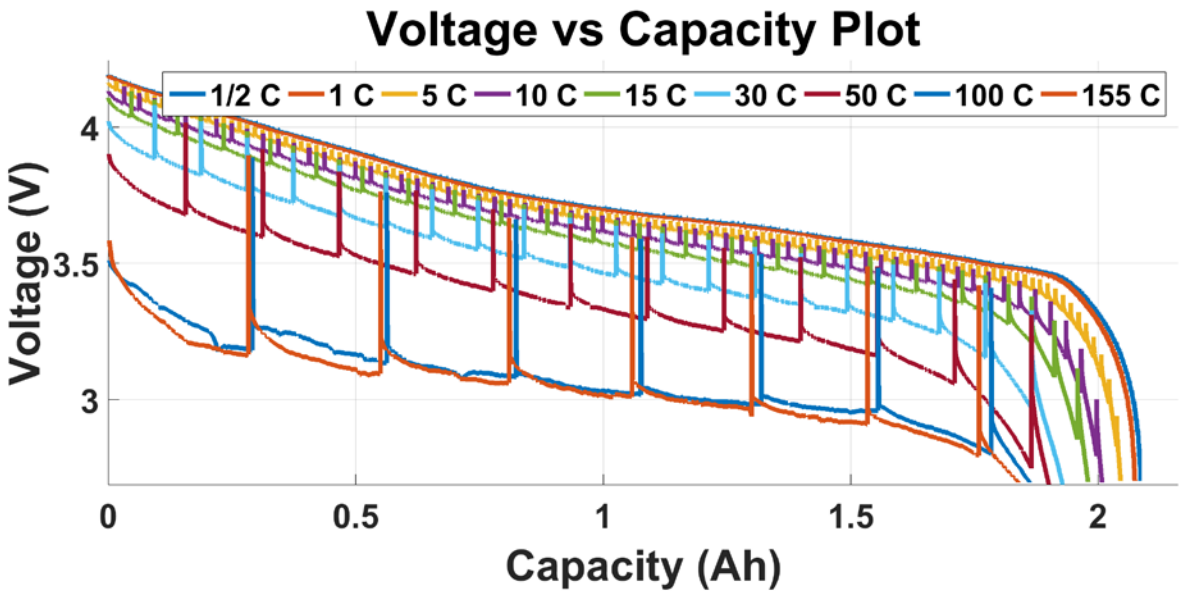


**Figure 27. SL2A 5s-1s Pulsed Discharge Voltage vs Capacity at Various Rates**

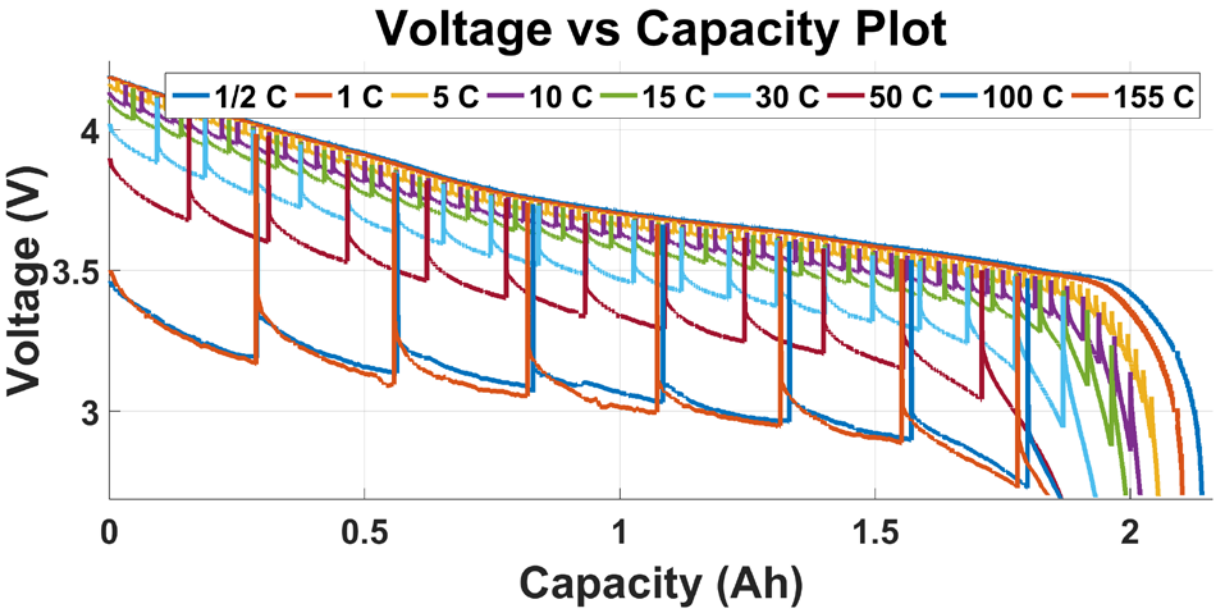


**Figure 28. SL2A 5s-5s Pulsed Discharge Voltage vs Capacity at Various Rates**

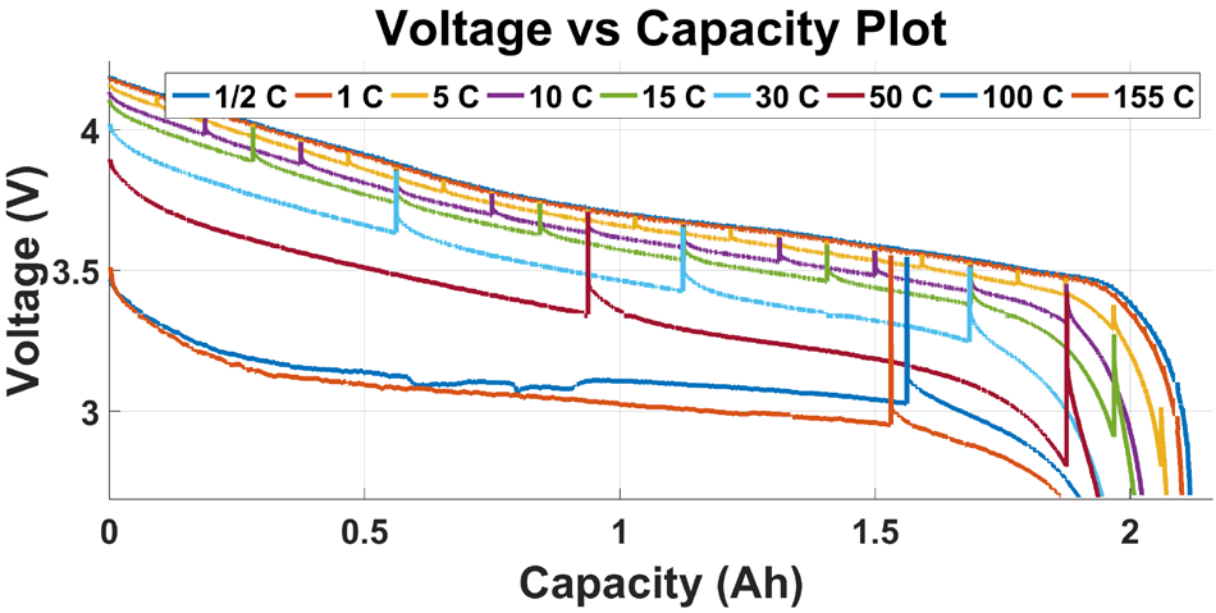


**Figure 29. SL2A 30s-5s Pulsed Discharge Voltage vs Capacity at Various Rates**

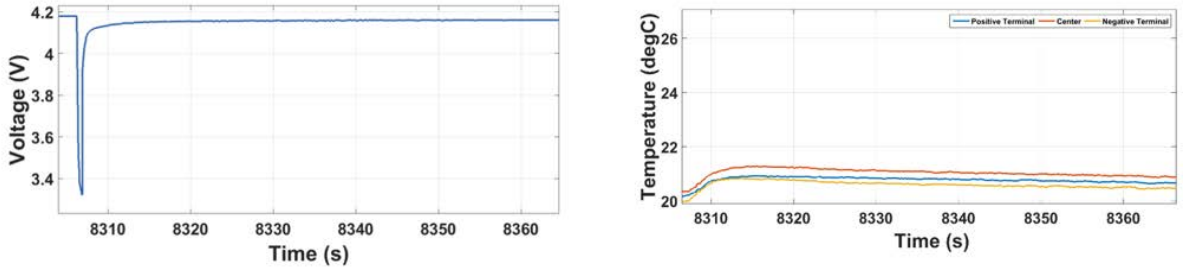


**Figure 30. Electrical (left) and Thermal (right) Data Collected when the Saft SL2A was Pulsed One Time at 225A in a 1 s Discharge / 59 s Rest Profile**

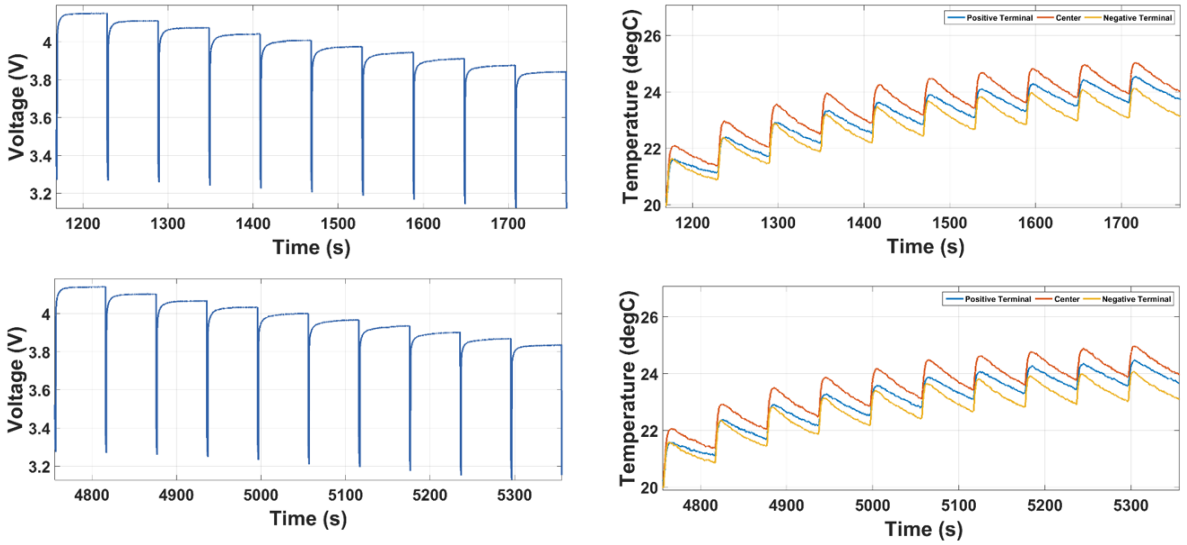


**Figure 31. Electrical (left) and Thermal (right) Data Collected when the Saft SL2A was Pulsed Ten Times at 225A in a 1 s Discharge / 59 s Rest Profile, Test #1 (above) and Test #2 (below)**

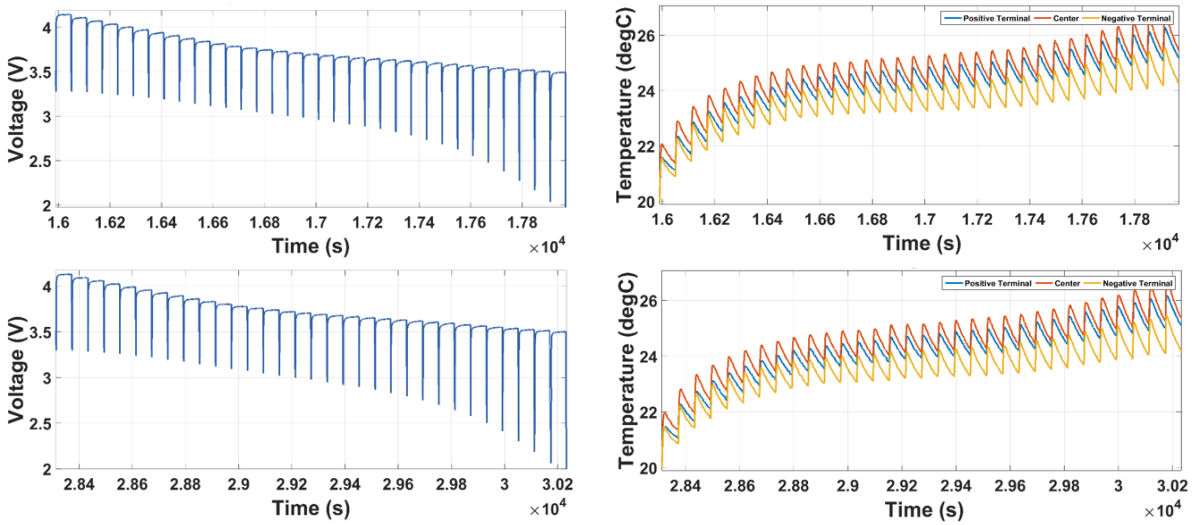


**Figure 32. Electrical (left) and Thermal (right) Data Collected when the Saft SL2A was Pulsed at 225A in a 1 s Discharge / 59 s Rest Profile Until the Cell Voltage Reached 2.0 V, Test #1 (above) and Test #2 (below)**

In summary, the Saft SL2A Deltran LIB performed very well under all rates evaluated. Unlike the Deltran battery, this is not all that surprising given that it is designed for pulsed power applications. Given its low capacity and high power density, this cell is well suited for use in high power applications that don't demand a great deal of energy from the prime power supply.

# 5.0 RESULTS AND DISCUSSION – MODELING

## 5.1 Deltran Model

It is desirable to have a circuit model of the Deltran battery that can be used to predict the behavior under both pulsed and continuous profiles. Most battery models use a voltage source along with a resistor-capacitor network to model the battery's behavior under different load conditions. A Deltran battery was cycled at various CC discharge rates from C/2 to 30C. The C/2 discharge is used to provide a stable voltage discharge curve for modeling the battery's open circuit voltage. Coupled using the battery's calculated state of discharge, curve-fitting techniques can be used to closely model the nonlinear nature of the battery's voltage based on the battery's current capacity, such as in Figure 33. For each battery that a model is developed for, its curve is defined by the sum of two exponential functions and a multi-order polynomial shown in Figure 34.

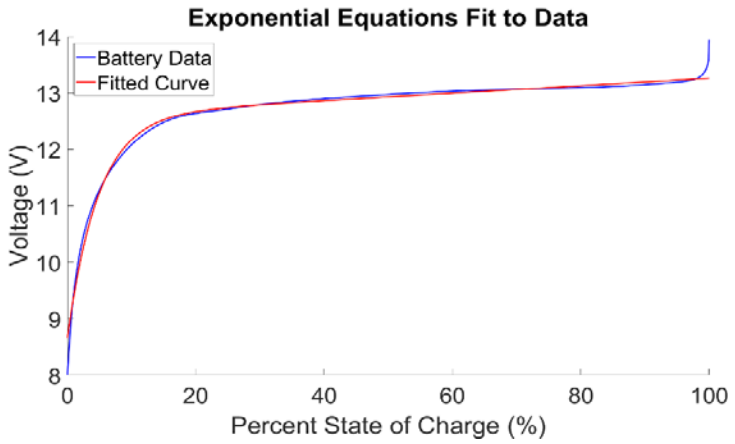


**Figure 33. Dual Exponential Functions Fit to the Battery Data**

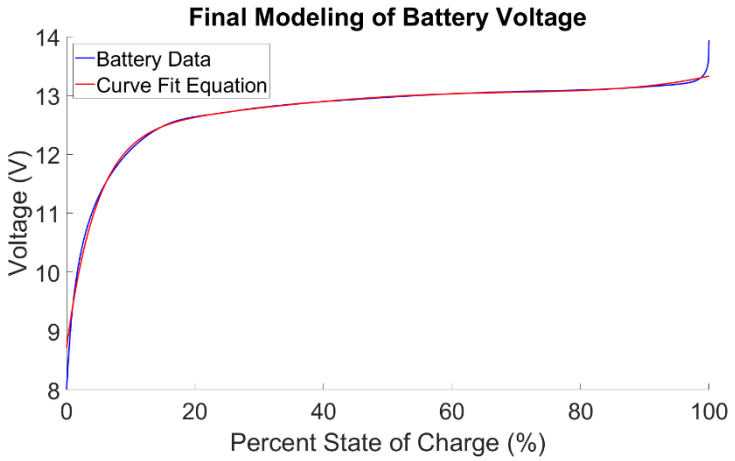


**Figure 34. Combined Exponential and Polynomial Equations to Better Fit the Battery Data**

By comparing higher C rate discharge curves to low C rate curves, the battery's ESR can be approximately calculated. Curves were generated that model the batteries apparent change in ESR based on the techniques described. For the best results, it was found that the overall ESR should be split in half with a large capacitor in parallel with one of the resistors. This capacitor provides a mechanism to reproduce the hysteresis effect seen in data. The use of behavioral sources in LTSpice is heavily used to implement the equations derived from the data. Equations are used to define voltage, SOC and also to act as decision trees that limit the battery from being infinitely charged, from acquiring negative capacity, etc. The model is presented visually in Figure 35 and some results from the model are presented in Figures 36 and 37, respectively. It should be noted that the basis for the models developed came from a shell of a model supplied by AFRL Kirtland and it was heavily modified and improved into the result shown here. The model operation is achieved as follows:

1. The user can set the initial capacity of the battery in Ah by altering the value of "AhInit" in the ".params" statement.
2. The behavioral voltage source labeled "Capacity" is used to calculate the capacity of the battery during simulation. The node labeled "VAHL" can be used to represent the battery's capacity in other behavioral source equations. As the model battery undergoes charging or discharging, the capacity of the battery is determined by integrating the current over time, initialized at the initial capacity. In addition, Limits are set so the battery cannot exceed full rated capacity or acquire negative capacity.
3. The capacity from the previous behavioral source is used to calculate the battery's current SOC. The calculated SOC is output on the behavioral source labeled "%SOC" at voltage node "vh".
4. The calculated SOC at node "vh" is then used in the behavioral voltage source "Voc" and the behavioral voltage sources "ESR" and "Transient" to output the model battery's open circuit voltage and resistive parameters, respectively. The result is the batteries voltage and apparent series resistance changing over time as the SOC changes.
5. Any desired load profile can be input to the system with the "Load Profile" voltage source. The output of this voltage source drives the current source "G1" to charge or discharge the model battery. Both charging and discharging can be done in the same simulation; however, the model will ignore any attempt to charge the battery above its rated capacity or below zero capacity. In this setup, positive values in a load profile charge the model battery and negative values in a load profile discharge the model battery.
6. Looking at voltage node "Vload" during simulation (positive terminal of the controlled current source) will show the terminal voltage of the battery as it is cycled.

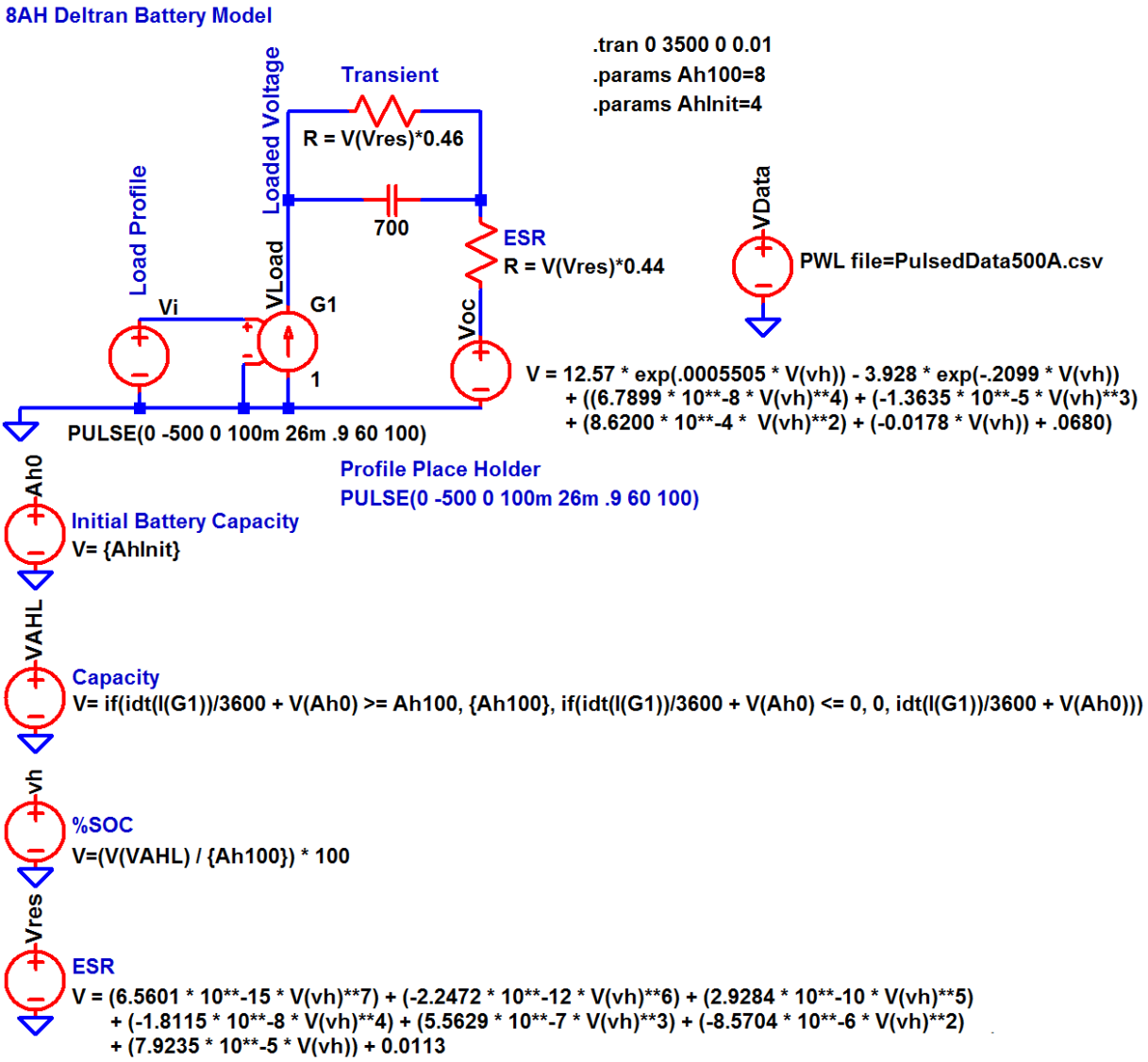


**Figure 35. Circuit Schematic of the Deltran Battery Model**

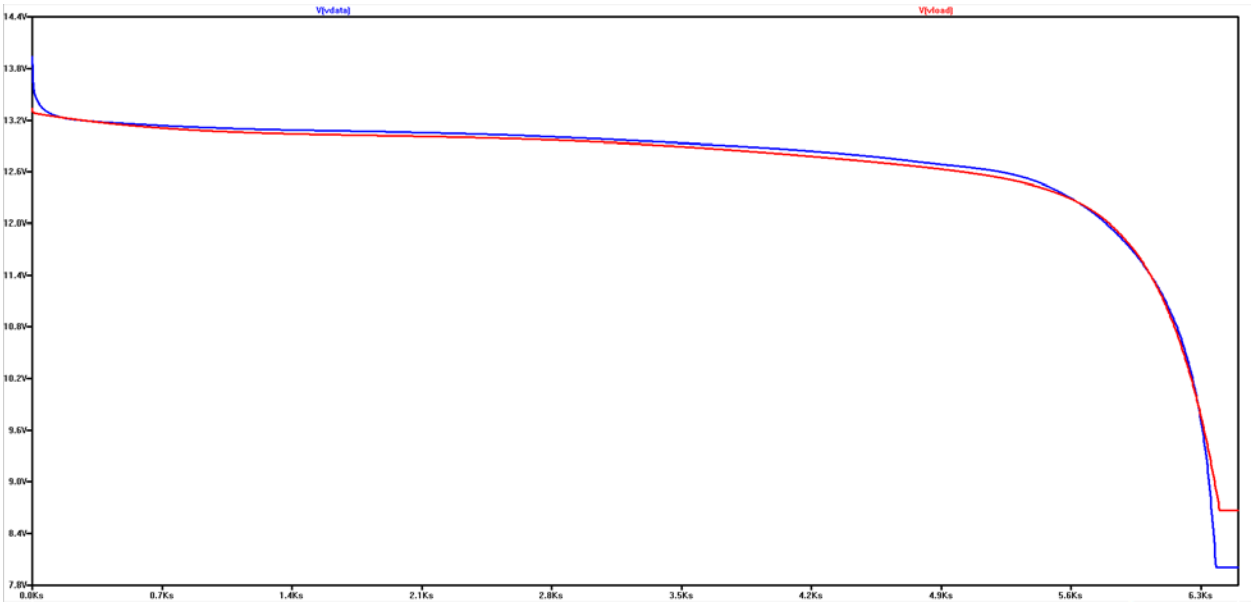


**Figure 36. Deltran 0.5C Discharge Data (blue) vs. 0.5C Discharge Simulation (red)**

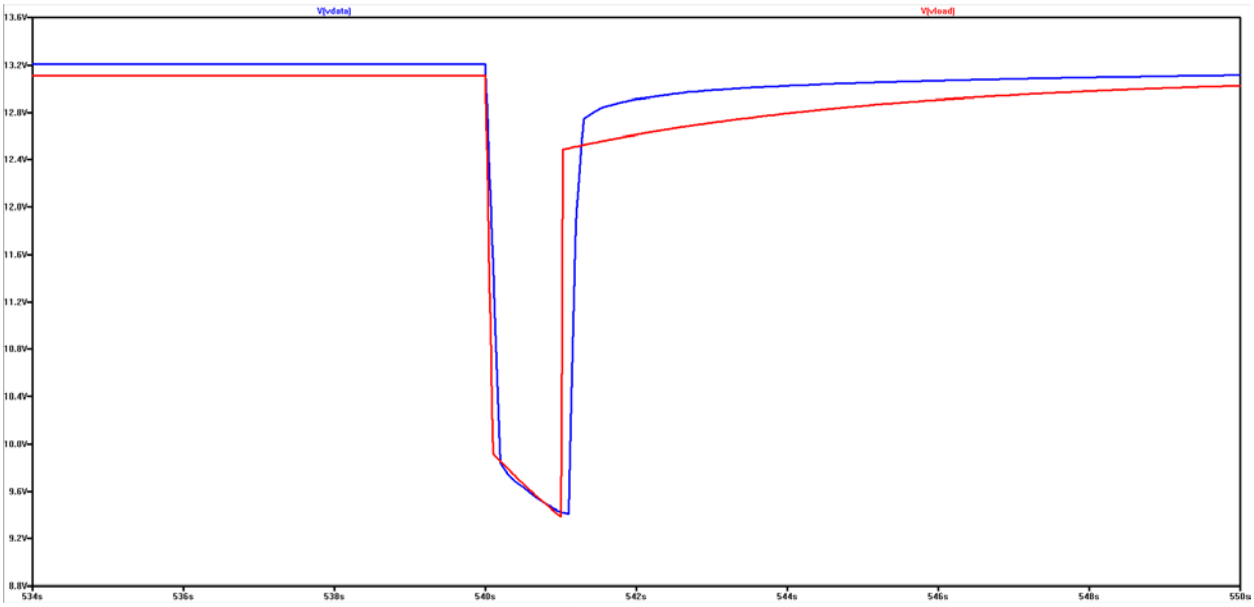


**Figure 37. Deltran 1s-59s 500A Pulse Discharge Data (blue) vs. 1s-59s 500A Pulse Discharge Simulation (red)**

## 5.2 SL2A Model

Similar to the Deltran module, the Saft SL2A pouch cell was cycled at different continuous discharge rates, shown above, in order to obtain equations that could be used as model parameters. A simulation model was developed in LTSpice for the Saft SL2A battery based on the Deltran model presented above. The model operates in the same way as described above with the only differences being adjustments to the equations describing the battery capacity limits, etc. This demonstrates how the model developed can be utilized for just about any battery if it is cycled properly and the correct equations obtained for input into

the model. The model developed for the SL2A cell is presented visually in Figure 38 and some sample results from the model are presented in Figures 39 and 40, respectively.

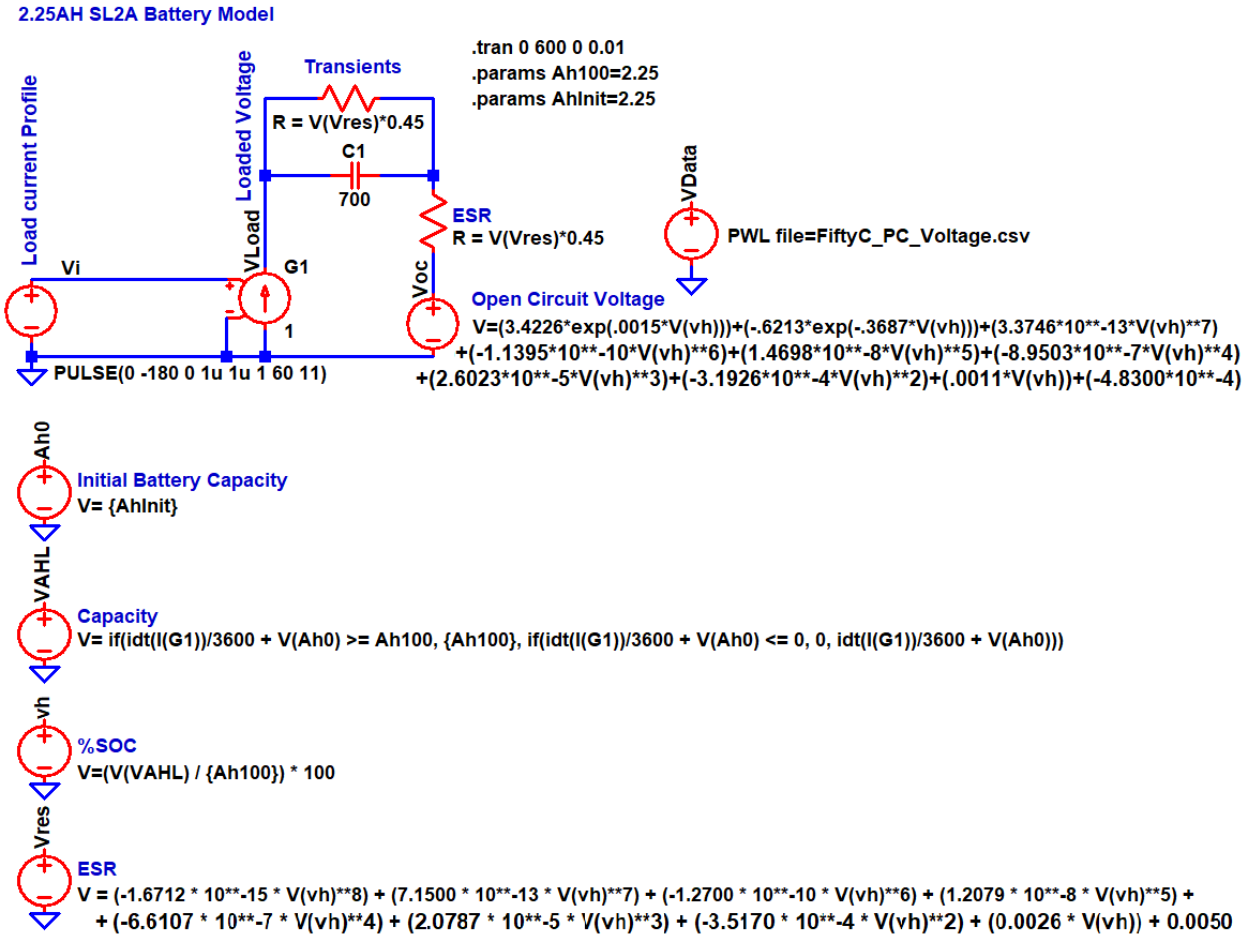


**Figure 38. Circuit Schematic of the SL2A Battery Model**

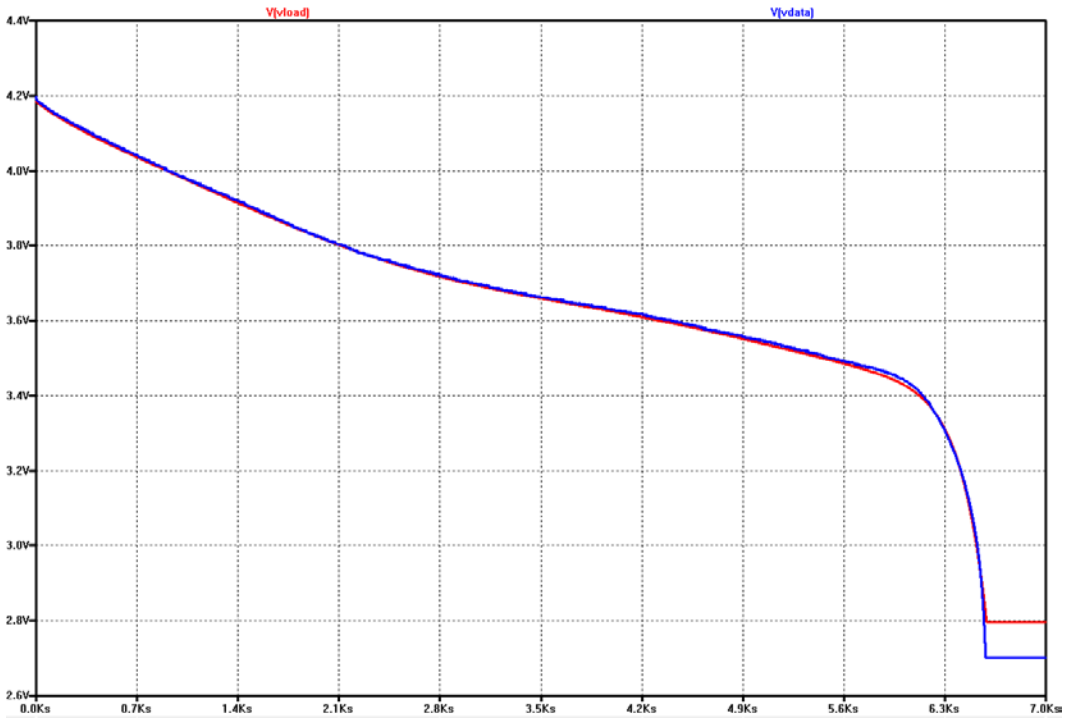


**Figure 39. SL2A 0.5C Continuous Discharge Experimental Data (blue) vs. 0.5C Continuous Discharge Simulation (red)**

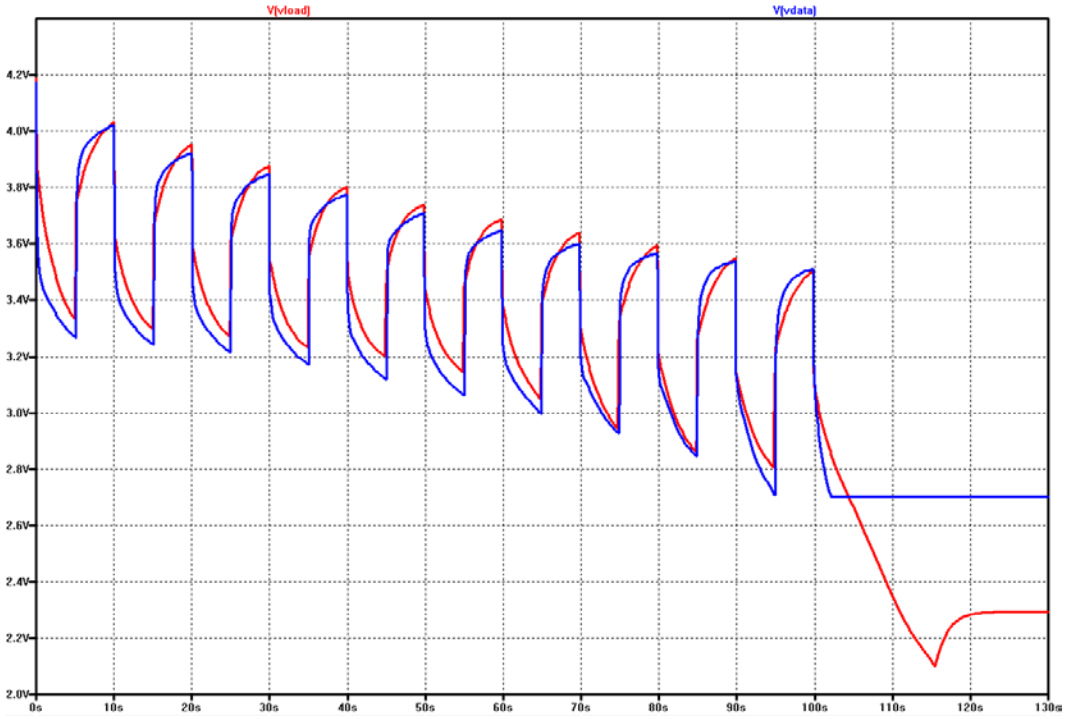


**Figure 40. SL2A 50C Pulsed Discharge Experimental Data (blue) vs. 50C Pulsed Discharge Simulation (red)**

## 6.0 PEM FUEL CELL BASICS

In the summer of 2015, AFRL provided UTA with a 110 cell, Ballard FCvelocity – 9SSL V4 20 kW PEM fuel cell [119], shown in Figure 41. Datasheet properties of the fuel cell are presented in Table 2. The basic operation of a PEM fuel cell is shown graphically in Figure 42. In a fuel cell the anode is the negative post of the fuel cell and it has several jobs. It conducts the electrons that are freed from the hydrogen molecules so that they can be used in an external circuit. It has channels etched into it that disperse the hydrogen gas equally over the surface of the catalyst. The cathode is the positive post of the fuel cell that has channels etched into it that distribute the oxygen to the surface of the catalyst. It also conducts the electrons back from the external circuit to the catalyst, where they can recombine with the hydrogen ions and oxygen to form water. The electrolyte or 'Proton Exchange Membrane' is a specially treated material that looks something like ordinary kitchen plastic wrap, only conducts positively charged ions. The membrane blocks electrons. For a proton-exchange membrane fuel cells (PEMFC), the membrane must be hydrated in order to function and remain stable. The catalyst is a special material that facilitates the reaction of oxygen and hydrogen. It is usually made of platinum nanoparticles very thinly coated onto carbon paper. The catalyst is rough and porous so that the maximum surface area of the platinum can be exposed to the hydrogen or oxygen. There are several steps involved with the operation of a PEM fuel cell. They are as follows:

1. Reaction Transport: Fuel is transported from storage to the anode. As long as fuel is supplied, reactions will take place.
2. Electrochemical Reaction: The fuel reacts with the anode plate liberating electrons from the electrode surface. Current related to how fast the reactions proceed so catalysts are used.
3. Ionic and Electronic Conduction: Liberated electrons flow through the conductive path and perform electrical work. The liberated ions travel through the electrolyte.
4. Product Removal: At least one product species created. (water, heat, etc.) Product must be removed but this is usually not a problem.

A fuel cell in essence works by breaking and forming bonds and using the energy conversion to produce electrical power. When bonds are formed, energy is released. When bonds are broken, energy is absorbed. For a reaction to result in the release of energy, formation of product bonds must be more than the energy absorbed to break reactant bonds. A fuel cell harvests the electrons as they go from higher energy reactant bonds to low energy product bonds. As shown in Figure 43, they are quite energy dense but not typically that power dense compared with other sources. The lack of power density stems from the time it takes the chemical reactions to occur and bonds to be broken and formed. The expected life of PEMFC is very short, 5,000 hours making it not really suitable for long term distributed generation. The most commonly used catalyst (Pt.) is very expensive and the most commonly used membrane, Nafion – a sulfonated tetrafluorethylene copolymer, is also very expensive. CO poisoning diminishes the efficiency since it tends to bind to Pt. thus, if CO is mixed with hydrogen, then the CO will take out catalyst space for the hydrogen. Hydrogen generation and storage is a significant problem. Despite these disadvantages, the ability to generate electricity in such a clean and energy dense manner is attractive and is worthy of studies like the one performed here.


**Figure 41. Ballard FCVelocity 9SSL Fuel Cell [119]**

**Table 2. Ballard FCVelocity 9SSL stack performance. Note that the 110 cell model was provided to UTA**

| Performance Parameter | | Current (A) | | | | | | | |
|---|---|---|---|---|---|---|---|---|---|
| | | 0 | 15 | 30 | 60 | 120 | 180 | 240 | 300 |
| 20 Cell Stack Average Gross Power – BOL | kW | 0.0 | 0.2 | 0.4 | 0.9 | 1.7 | 2.5 | 3.2 | 3.8 |
| 25 Cell Stack Average Gross Power – BOL | kW | 0.0 | 0.3 | 0.6 | 1.1 | 2.2 | 3.2 | 4.1 | 4.8 |
| 55 Cell Stack Average Gross Power – BOL | kW | 0.0 | 0.7 | 1.3 | 2.5 | 4.8 | 7.0 | 9.0 | 10.6 |
| 71 Cell Stack Average Gross Power - BOL | kW | 0.0 | 0.9 | 1.8 | 3.4 | 6.3 | 9.1 | 11.6 | 13.7 |
| 75 Cell Stack Average Gross Power – BOL | kW | 0.0 | 0.9 | 1.8 | 3.5 | 6.6 | 9.6 | 12.3 | 14.4 |
| 90 Cell Stack Average Gross Power – BOL | kW | 0.0 | 1.1 | 2.2 | 4.2 | 8.0 | 11.5 | 14.7 | 17.3 |
| 110 Cell Stack Average Gross Power – BOL | kW | 0.0 | 1.4 | 2.7 | 5.1 | 9.7 | 14.1 | 18.0 | 21.2 |
| Average Cell Voltage – DV Testing BOL Minimum (Hydrogen Up and Down Polarization according to the conditions of Table 2) | V | 0.965 | 0.857 | 0.825 | 0.788 | 0.742 | 0.715 | 0.683 | 0.643 |
| Individual Cell Voltage differential below Average Cell Voltage - BOL maximum | V | 0.030 | 0.030 | 0.030 | 0.030 | 0.030 | 0.030 | 0.050 | 0.080 |
| Individual Cell Voltage Decay | µV/hr | Determined by Operating Conditions and Load Profile | | | | | | | |
| Lifetime | hours | Determined by Operating Conditions and Load Profile | | | | | | | |

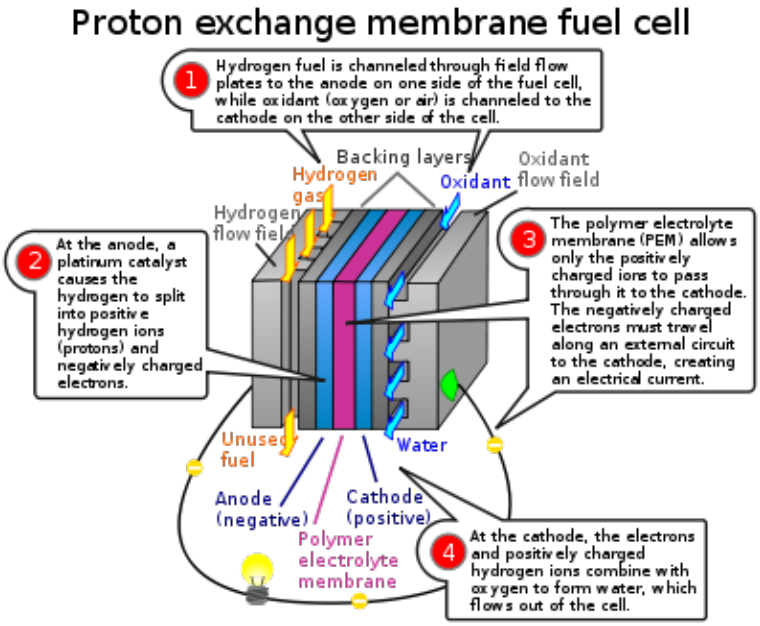


**Figure 42. PEM Fuel Cell Operation [120]**

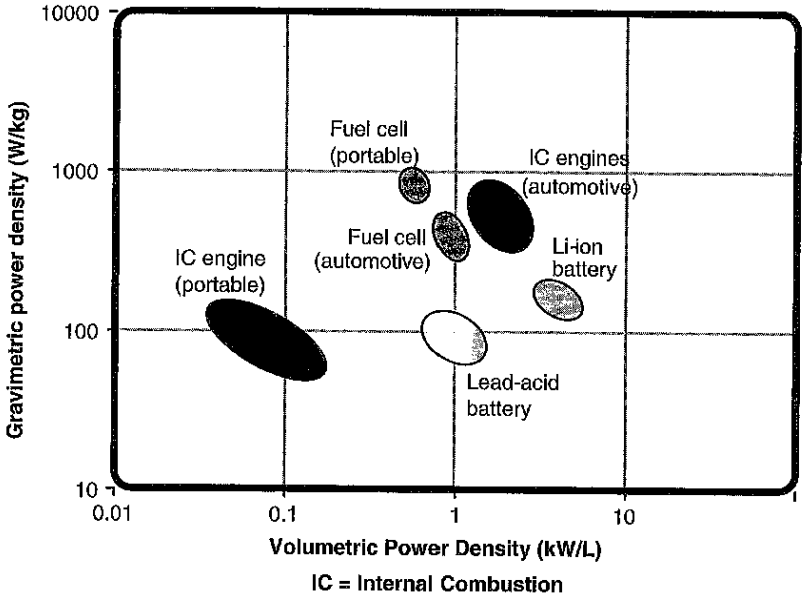


**Figure 43. Fuel Cell Power and Energy Density [121]**

## 6.1 Fuel Cell Accomplishments in FY16/FY17

Along with the fuel cell, AFRL also provided a suggested schematic layout for setting up the Ballard fuel cell in an operational state. The provided schematic is shown in Figure 44. UTA began working with AFRL Kirtland to obtain and specify all of the supporting components found in the drawing that are required for operation of the fuel cell. Several components were provided by AFRL with anticipation that they may be able to be used in some instances and UTA was directed to obtain quotes for procurement of the remaining parts. Obtaining quotes turned out to be a very difficult task given the high flow rates of $H_2$ and Air. Additionally, many vendors refused to quote the requested parts since they would be utilized with $H_2$, which is of course a very flammable gas if not properly handled. As a response to these struggles, UTA reached out to Ballard for suggested vendors and part numbers that could be utilized to bring the fuel cell into an operational state.

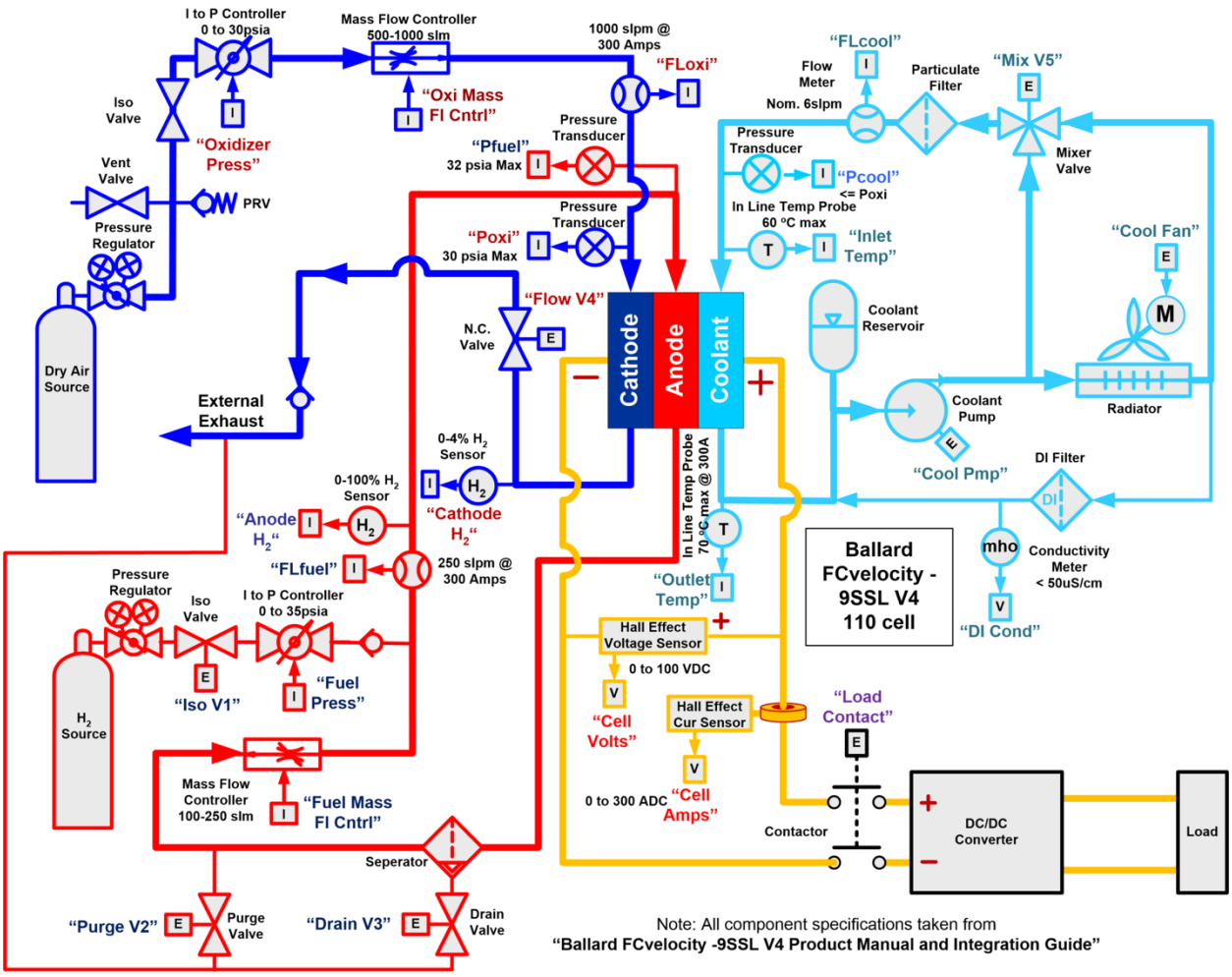


**Figure 44. Schematic Diagram of the Proposed Ballard Fuel Cell Setup Provided by AFRL**

Ballard reviewed the drawing shown in Figure 44 and explained that many components within the drawing were either not needed or were incorrectly specified. In late August 2016, Ballard provided UTA with schematic diagram they had previously used to get this family of fuel cells operational. That drawing is shown in Figure 45, which is still missing an intercooler element that is required on the cathode input side since an air compressor is being utilized that will heat up the air source considerably. To protect the fuel cell membrane, the hot air must be cooled and an inline intercooler must be used at the cathode input.

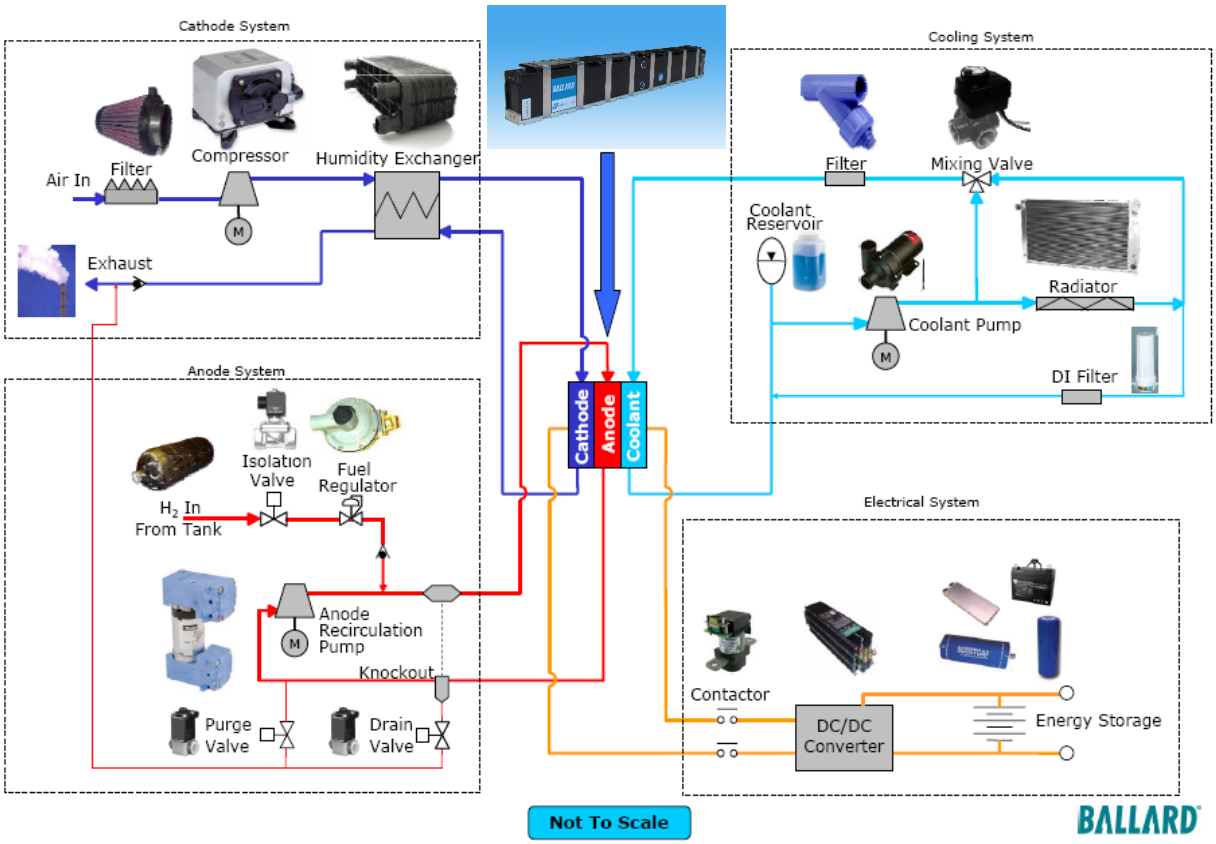


**Figure 45. Schematic Diagram of the Proposed Ballard Fuel Cell Setup. The Drawing is Provided by Ballard**

UTA proceeded to obtain quotes from various manufacturers to update the bill of materials (BOM) as shown in Table 3. Several components in the BOM require special order and some even require permission from Ballard to purchase since they were at one time manufactured for them. The compressor and recirculation pump were among those that require Ballard approval for purchase. The BOM below was provided to AFRL in September of 2017 and at the time of this writing many parts are still in the process of being procured. A description of each item shown in Figure 45 and listed in Table 3 is provided below.

**Table 3. Fuel Cell Supporting Hardware BOM Based Upon the Ballard Provided Schematic**

| Item | Company | Item# | QTY | Price (Each) | Price Total | Quote | Data-Sheet |
|---|---|---|---|---|---|---|---|
| **Cathode** | | | | | | | |
| Compressor | Air Squared | P34 | 1 | $4,450 | $4,450 | Yes | Yes |
| Air filter | Filter Freudenburg | FC-F-0514-N | 1 | $410.75 | $411 | Yes | Yes |
| Intercooler | Bell Intercoolers | W450025060UTA02 | 1 | $505.80 | $506 | Yes | Yes |
| Humidifier | FuMATech | 2017O000716 | 1 | $5318.97 | $5319 | Yes | Yes |
| **Anode** | | | | | | | |
| Hydrogen Recirculation Pump | KNF | PU3773 - N838.1.2 | 2 | $1,383.80 | $2,768 | Yes | Yes |
| Purge Valve | Burkert | 00298112 | 1 | $417.64 | $418 | Yes | Yes |
| Isolation/ Pressure relief Valve | Burkert | 00304642 | 2 | $383.72 | $768 | Yes | Yes |
| Biasing Pressure Regulator | Tescom | 44-4069E212 | 1 | $2,403.00 | $2,403 | Yes | Yes |
| Needle Valve | Swagelocke | SS-1RS8 | 1 | $95.40 | $96 | Yes | Yes |
| **Cooling System** | | | | | | | |
| Pump | Cummins | 1030002232PA02 | 1 | $466.66 | $467 | Yes | No |
| Radiator | Bell Intercoolers | R150185185UTA01 | 1 | $1,032.30 | $1,032 | Yes | Yes |
| Mixing Valve | Fluid Power Energy | AL1010PVW1-130 | 1 | $190.00 | $190 | Yes | Yes |
| Temperature Sensors | Omegadyne | TC-T-NPT-G-72 | 3 | $40.00 | $120 | Yes | Yes |
| Mass Flow Meter | UTA already owned equipment | | | | | N/A | N/A |
| DI Filter | UTA already owned equipment | | | | | N/A | N/A |
| Coolant Reservoir | UTA already owned equipment | | | | | N/A | N/A |
| **System Instrumentation** | | | | | | | |
| Hydrogen Sensor (Cathode 0 -4%) | Mouser | HLS-440P A | 1 | $980.12 | $980 | Yes | Yes |
| Hydrogen Sensor (Anode 0-100%) | EIS | HPS-100 | 1 | $913.85 | $914 | Yes | Yes |
| Pressure Sensor | Omegadyne | PX219-100A5V | 4 | $265.00 | $1060 | Yes | Yes |
| Ground Fault Test | Bender | IR425-D4-1 | 1 | $734.00 | $734 | Yes | Yes |
| **Connections and Tubing (Swagelok)** | | | | | | | |
| Tubing | Silflex | C3/17/1000,C3/20/1000, C3/24/1000 | 1 | $26.22 | $26 | Yes | Yes |
| Tubing Connectors | McMaster | | | | | | |
| | | | | | | | |
| | | | | Total: | $22,562 | | |

## 6.2 Fuel Cell Supporting Hardware

This section will review the required components from the three categories in the Ballard schematic: Cathode, Anode and Cooling.

Cathode Hardware

The cathode input utilizes compressed air to provide oxygen for the fuel cell reaction process. To accomplish this a scroll compressor is utilized. Dry air is dangerous to the membrane of the fuel cell; therefore, a humidifier must be used to increase water content in the dry air. Special humidifier designs made specifically for fuel cells utilized the exhaust product of water to increase water content in the dry air.

Compressor

To meet the pressure and flow requirements for the Ballard fuel cell, a specialty compressor would need to be obtained. This fuel cell selected is an Air Squared P34. This compressor was designed for Ballard and their higher-powered fuel cells. To purchase this component Ballard approval is required, which UTA obtained previously.

Air Filter

The air filter is a simple paper filter to remove containments before the scroll compressor. To meet the flow requirements a Freudenburg filter P/N# FC-F-05140N was selected, which was recommended by Ballard.

Intercooler

To protect the membrane of the fuel cell, hot air from the compressor must be cooled before going into the cathode of the fuel cell. This intercooler was designed by Bell Intercoolers and a variety of connection ports could be made for any application. The base intercooler is a COTS component and Bell Intercooler would be welding on the connections. A drawing was given to UTA with drawing # W450025060UTA02.

Humidifier

To protect the membrane of the fuel cell, dry air must be humidified before being inputted into the cathode port. Typical fuel cell humidifiers are specialty designed and are often the most expensive component for the supporting hardware. This is especially the case when the fuel cell requires a very high flow rate. The water content is provided from the exhaust output. The humidifier chosen was one produced by FuMATech.

Cathode Hydrogen Sensor

A hydrogen sensor with a range of 0-4% is placed before the Cathode input to determine if any leaks are occurring at the fuel cell. If the hydrogen content goes out of range an alarm will trigger to shut down the fuel cell. For this application a sensor from Applied Sensor P/N# HLS-440P A was chosen. One of these sensors is available on Mouser since it is a discontinued part and no longer sold from Applied Sensor.

Anode Hardware
The anode input utilizes compressed hydrogen for the fuel cell reaction process. Several regulators are required to maintain anode to cathode pressure deltas. The recirculation pumps are used to increase efficiency.

Hydrogen Recirculation Pump
During the fuel cell reaction, not all the Hydrogen passing the membrane is utilized. To increase efficiency, unused Hydrogen is recirculated back to the input of the anode. To accomplish this two KNF PU3773 - N838.1.2 is utilized. This pump is another Ballard special design, which requires Ballard approval for purchase. UTA received permission from Ballard to purchase the pump.

Purge Valve
The purge valve removes any air or water in the anode output before being recirculated into the hydrogen source. Special care must be taken, as purged hydrogen becomes a safety risk. A Burkert 00298112 is used to purge the air.

Biasing Pressure Regulator
The biasing pressure regulator maintains the optimal pressure difference between the cathode and anode input. The fuel cell requires a specific pressure differential to operate. To maintain this pressure regulation a Tescom 44-4069E212 is utilized.

Anode Hydrogen Sensor
The anode hydrogen sensor monitors the hydrogen concentration in the Hydrogen line. This component ensures proper operation of the fuel cell. The sensor used is an Applied Sensor HPS-100. This component is discontinued from the manufacturer but the part was located on EIS for purchase.

Needle Valve
The needle valve will be implemented to follow after the purge valve. A Swagelocke SS-1RS8 is component that will be used to do this.

Isolation/Pressure Relief Valve
The isolation valve is located between the hydrogen tank and the fuel regulator. This will be used to isolate the hydrogen tank from the rest of the anode system. The pressure relief valve will be used to relieve pressure if there is too much. A Burkert 00304642 will be used for both of these applications.

Cooling Hardware
The cooling hardware is required to prevent the fuel cell from overheating.

Pump
A simple coolant pump from Cummins (P/N#1 030002232PA02) is used to flow coolant.

Radiator
Bell Intercoolers also designed the radiator to cool the coolant liquid. Bell Intercoolers provided a drawing # R150185185UTA01.

Mixing Valve
The mixing valve is used to maintain the optimal fuel cell temperature. A mixing valve from Fluid Power Energy (P/N # Al1010PVW1-130) is used.

DI filter
The DI filer will be to filter out any impurities in the cooling system. This will be provided by UTA.

Coolant Reservoir
The coolant reservoir will be where the coolant will be stored prior to being pumped through the system. This component is provided by UTA.

Temperature Sensors
Three temperature sensors will be used to monitor the coolant in, coolant out and on the cathode out. These will be from Omegadyne and have T-type thermocouple connections.

Mass Flow Meter
This will be used to measure the oxidant flow that is going into the compressor. This unit is already owned by UTA.

Other System Components
These components are not specifically in any of the other system but still pertain to the whole fuel cell system.

Ground Fault Test
The ground fault test will be used to cut off power to the device if it detects an issue. The Bender IR425-D4-1 will be used for this purpose.

Pressure Sensor
The pressure sensor will be used to monitor the pressure on the anode in, anode out, cathode in and cathode out portions of the fuel cell. Four Omegadyne Px219-100A5V will be used for this.

Tubing and Connectors
The tubing will be a variation of 17mm, 20mm and 24mm. This tube will be used to connect all components in each system together. Since each component has different size outlets and inlets connectors will be used to join the different sized ends together.

## 7.0 CONCLUSIONS

The results of this work have shown that lithium-ion batteries possess significant energy and power density that make them quite feasible for use in electric vehicles, electric grids and for driving high power Marx generators for AFRL applications. Two different COTS batteries have been cycled and models have been developed and experimentally validated using the experimental data. A 20 kW Ballard fuel cell has been studied and the requirements for making it operational have been completed. A BOM has been supplied to AFRL Kirtland and at the time of this writing, September 2017, UTA is still working with AFRL Kirtland to procure the supporting components needed to setup and evaluate the Ballard fuel cell. It is anticipated that this will be completed in the next few months and the fuel cell will be evaluated in the spring of 2018.

## 8.0 RECOMMENDATIONS

The recommendations are that AFRL Kirtland continue to pursue and study lithium-ion batteries for use in its future fleet and that UTA will continue to work with AFRL Kirtland to secure the parts needed to evaluate the 20 kW Ballard fuel cell under high power load conditions.

## 9.0 REFERENCES


1. S.D. Korovin, V.V. Rostov, S.D. Polevin, I.V. Pegel,E. Schamiloglu, M.I. Fuks, and R.J. Barker, 'Pulsed Power-Driven High-Power Microwave Sources,' Proceedings of the IEEE, Vol. 92, No. 7, July 2004, pp. 1082 – 1095.
2. E. Schamiloglu, 'High Power Microwave Sources and Applications,' IEEE MTT-S Digest, 2004, pp. 1001 – 1004.
3. X. Chen, Virtual Cathode Oscillator as High Power Microwave Source, VDM Verlag, 2008.
4. Y.J. Chen, A.A. Neuber, J.J. Mankowski, J.C. Dickens, M. Kristiansen, R. Gale, 'Design and Optimization of a Compact, Repetitive, High-Power Microwave System,' Review of Scientific Instruments, Vol. 76, No. 10, Oct 2005.
5. AFRL Directed Energy Directorate, 'Briefing to Request for Information,' http://www.wslfweb.org/docs/usg/de.pdf, [Online], February 14, 2000.
6. AFRL Directed Energy Directorate, 'Directed Energy Directorate,' http://www.kirtland.af.mil/afrl_de/, [Online], December 31, 2014.
7. J. Walters, J. Dickens, M. Kristiansen, 'An "Energy Efficient" Vircator-Based HPM System,' Proceedings of the 2011 IEEE International Pulsed Power Conference (PPC), 2011, pp. 658 – 661.
8. C. Wilson,' High Altitude Electromagnetic Pulse (HEMP) and High Power Microwave (HPM) Devices: Threat Assessments,' Naval History & Heritage Command, http://www.history.navy.mil/library/online/hemp_hpm.htm, [Online], December 14, 2014.
9. 'USAF's CHAMP Missile Completes First Weapons Test Flight,' ©2015 Kable,, http://www.airforce-technology.com/news/newsusaf-champ-missile, [Online], December 31, 2014.
10. Staff Sgt. D. Suits, 'AFRL Commander Describes Air Force's Technology Vision,', Air Force News Service, September 16, 2014, http://www.af.mil/News/ArticleDisplay/tabid/223/Article/497459/afrl-commander-describes-air-forces-technology-vision.aspx, [Online] December 31, 2014.
11. H.D. Fair, 'Advances in Electromagnetic Launch Science and Technology and Its Applications,' IEEE Transactions on Magnetics, Vol. 45, No. 1, Part 2, 2009, pp. 225 – 230.
12. Electromagnetic Railgun, http://www.onr.navy.mil/media-center/fact-sheets/electromagnetic-railgun.aspx, Office of Naval Research (ONR), [Online], December 14, 2014.
13. Allen, Raymond; Neri, Jesse, "A Battery Powered, 200-KW Rapid Capacitor Charger for a Portable Railgun in Burst Mode Operation at 3 RPS," Plasma Science, 2007. ICOPS 2007. IEEE 34th International Conference on , vol., no., pp.867,867, 17-22 June 2007.
14. A. Sitzman, D. Surls, and J. Mallick, 'Design, Construction, and Testing of an Inductive Pulsed-Power Supply for a Small Railgun,' IEEE Trans. on Magnetics, Vol. 43, No. 1, pp. 270 – 274, January 2007.
15. Wells, B.T.; Stevenson, R.C.; McElroy, J.; Noh, J.; Ramadoss, S.; Gunow, G.A.; Hammig, M.D., "Defeating IEDs, SNM and contraband secreting via long range gamma-ray imaging of neutron interrogated materials," Nuclear Science Symposium Conference Record (NSS/MIC), 2009 IEEE , vol., no., pp.668,675, Oct. 24 2009-Nov. 1 2009.

16. R. O'Rourke, 'Navy Shipboard Lasers for Surface, Air, and Missile Defense: Background and Issues for Congress,' Congressional Research Service, 7-5700, www.crs.gov, R41526, July 31, 2014.
17. Solid-State Laser Technology Maturation Program, http://www.onr.navy.mil/Media-Center/Fact-Sheets/Solid-State-Laser-Technology-Maturation-Program.aspx, [Online], December 14, 2014.
18. D. Smalley, 'Historic Leap: Navy Shipboard Laser Operates in Persian Gulf,' http://www.onr.navy.mil/Media-Center/Press-Releases/2014/LaWS-shipboard-laser-uss-ponce.aspx, [Online], December 31, 2014.
19. 'Boeing YAL-1,' http://en.wikipedia.org/wiki/Boeing_YAL-1, [Online], December 31, 2014.
20. Jang, S.R.; Ryoo, H.J.; Jin, Y.-S.; Ahn, S.H.; Rim, G.-H., "Application of pulsed power system for water treatment of the leachate," Pulsed Power Conference, 2009. PPC '09. IEEE, vol., no., pp.980,983, June 28 2009-July 2 2009.
21. Ronny Brandenburg, Hana Barankova, Ladislav Bardos, Andrzej G. Chmielewski, Miroslaw Dors, Helge Grosch, Marcin Hołub, Indrek Jõgi, Matti Laan, Jerzy Mizeraczyk, Andrzej Pawelec and Eugen Stamate (2011). Plasma-Based Depollution of Exhausts: Principles, State of the Art and Future Prospects, Monitoring, Control and Effects of Air Pollution, Prof. Andrzej G. Chmielewski (Ed.), ISBN: 978-953-307-526-6, InTech, Available from: http://www.intechopen.com/books/monitoring-control-and-effects-of-air-pollution/plasmabased- depollution-of-exhausts-principles-state-of-the-art-and-future-prospects.
22. A Khacef1, J M Cormier and J M Pouvesle, 'NOx Remediation in Oxygen-Rich Exhaust Gas Using Atmospheric Pressure Non-Thermal Plasma Generated by a Pulsed Nanosecond Dielectric Barrier Discharge,' Journal of Physics D: Applied Physics Volume 35 Number 13, 2002.
23. J.A. Gaudet, R.J.Barker, C.J. Buchenauer, C. Christodoulou, J. Dickens, M.A. Gundersen, R.P. Joshi, H.G. Krompholz, J.F. Kolb, A. Kuthi, M. Laroussi, A. Neuber, W. Nunnally, E. Schamiloglu, K.H. Schoenbach, J.S. Tyo, R.J. Vidmar, 'Research Issues in Developing Compact Pulsed Power for High Peak Power Applications on Mobile Platforms,' Proceedings of the IEEE,Vol. 92 , No. 7, 2004, pp. 1144 – 1165.
24. Schamiloglu, E.; Schoenbach, K.H.; Vidmar, R.J., 'On the Road to Compact Pulsed Power: Adventures in Materials, Electromagnetic Modeling, and Thermal Management,' 14th International IEEE Pulsed Power Conference, Vol. 1, 2003, pp. 3 – 8.
25. G. Sarre, P. Blanchard, M. Broussely, 'Ageing of Lithium-Ion Batteries,' Journal of Power Sources, Vol. 127, Issues 1-2, March 2004, pp. 65-71.
26. Y. Chen, A. Sitzman, 'Testing a Lithium-ion Battery as a Pulsed Power Source,' 15th IEEE International Pulsed Power Conference, Monterey, California, June 13-17, 2005.
27. J. Li, E. Murphy, J. Winnick, P.A. Kohl, 'Studies on the Cycle Life of Commercial Lithium-ion Batteries During Rapid Charge-Discharge Cycling,' Journal of Power Sources, No 102, pp 294-301, 2001.
28. J. Lopez, M Gonzalez, J.C. Viera, and C. Blanco, "Fast-Charge Lithium-Ion Batteries for Portable Applications," 26th Annual International Telecommunications Energy Conference, Chicago, IL, September 19-23, 2004.
29. G. Ning, B. Haran, and B.N. Popov, J. Power Sources, 117, p. 160–169 (2003).
30. Vetter, J., and et. al., J. of power sources, 147, p. 269 – 281 (2005).
31. J.-M. Tarascon and M. Armand, 'Issues and Challenges Facing Rechargeable Lithium Batteries,' Nature, Vol. 414, pp. 359 – 367, November 2001.

32. J.B. Goodenough, 'Cathode Materials: A Personal Perspective,' Journal of Power Sources, Vol. 174, No. 2, pp. 996-1000, December 2007.
33. Saft Americas, Lithium-Ion Battery Technologies, http://www.saftbatteries.com/Technologies_Lithium_Liion_301/Language/en-US/Default.aspx, July 15, 2011, Copyright © Saft 2007.
34. Data sheet for the Saft VL 5U - Ultra high power cell, Saft America, Inc., Space & Defense Division, Doc N° 54073-2-1009, Edition: October 2009, www.saftbatteries.com.
35. Lithium Technology Corporation, http://www.gaia-akku.com/en/products/cells.html, ©2013 LTC | 10379B Democracy Lane, Fairfax, Virginia 22030, USA, [Online], December 31, 2014.
36. Lithium-ion Cells and Batteries, http://yardney.com/msds/li-ion/lithium-ion-cells-and-batteries/ ,© 2014 Yardney Technical Products, [Online], December 31, 2014.
37. Lithium-ion Batteries, http://www.eaglepicher.com/technologies/battery-power/lithium-ion-liion, Copyright © 2013 EaglePicher Technologies, [Online], December 31, 2014.
38. K2 Energy Solutions, Inc, http://www.k2battery.com/, [Online], December 31, 2014.
39. DOW Kokam Lithium-ion Batteries, http://dev.dowkokam.com/tech-cells.htm, [Online], December 31, 2014.
40. Deltran Lithium-ion Lead Acid Replacement Battery, http://www.batterytender.com/, Deltran Battery Tender®, © 2014, February 26, 2015.
41. D.A. Wetz, B. Shrestha, P. Novak, and Y. Chen, 'Cycling of Electrochemical Energy Storage Devices at Elevated Rates,' Journal of Directed Energy, Vol. 4, No. 4, pp. 211 – 231, Summer 2012.
42. D.A. Wetz, B. Shrestha, and P. Novak, 'High Power Electrochemical Energy Storage for Directed Energy Applications,' SAE Int. J. Passeng. Cars – Electron. Electr. Syst., Vol.6, No. 1, May, 2013.
43. D.A. Wetz, B. Shrestha, and P. Novak, 'Elevated Rate Cycling of High Power Electrochemical Energy Storage Devices for Use as the Prime Power Source of an EM Launcher,' IEEE Transactions on Plasma Science, Vol. 41, No. 5, pp. 1319 – 1325, May, 2013.
44. D.A. Wetz, B. Shrestha, and P.M. Novak, 'Pulsed Evaluation of High Power Electrochemical Energy Storage Devices,' IEEE Transactions on Dielectrics and Electrical Insulation, Vol. 20, No. 4, pp. 1040 – 1048, August, 2013.
45. D.A. Wetz, B. Shrestha, P. Novak, and Y. Chen, 'Characterization of High Power Electrochemical Energy Storage Devices for use in Naval Applications,' Naval Engineers Journal, Vol. 125, No. 3, pp. 125 – 135, September 2013.
46. D.A. Wetz, P.M. Novak, B. Shrestha, J.M. Heinze1, and S.T. Donahue, 'Electrochemical Energy Storage Devices in Pulsed Power,' IEEE Transactions on Plasma Science, Vol. 42, No. 10, Part 2, pp. 3034 – 3042, October, 2014.
47. D.A. Wetz, B. Shrestha, S.T. Donahue, D.N. Wong, M.J. Martin, and J.M. Heinzel, 'Capacity Fade of 26650 Lithium-Ion Phosphate Batteries Considered for use within a Pulsed Power System's Prime Power Supply,' Submitted for review to the IEEE Transactions on Plasma Science in October 2014, pending review.
48. B. Shrestha, D.A. Wetz, and P. Novak, 'Pulsed Elevated Rate Discharge of Electrochemical Energy Storage Devices,' IEEE Transactions on Plasma Science, Vol. 40, No. 10, Part: 1, pp. 2462 – 2469, October, 2012.
49. B.M. Huhman, J.M. Neri, and D.A. Wetz, 'Application of a Compact Electrochemical Energy Storage to Pulsed Power Systems,' IEEE Transactions on Dielectrics and Electrical Insulation, Vol. 20, No. 4, pp. 1299 – 1303, August 2013.

50. Ryan O'Hayre, et. Al., Fuel Cell Fundamentals 2nd Edition, John Wiley and Sons, Inc., © 2009, Hoboken, New Jersey. ISBN: 978-0-470-25843-9.
51. James Larminie, et. Al., Fuel Cell Systems Explained 2nd Edition, John Wiley and Sons, Inc., © 2003, West Sussex, England, ISBN:0-4700-84857-X.
52. Ballard Power Systems, http://www.ballard.com/, © 2013 Ballard Power Systems Inc., February 26, 2015.
53. Ra, Issac., "Evolution of rechargeable lithium-ion battery," International workshop energy storage technologies and application, ABD, Apr. 3, 2013.
54. R. Chandrasekaran, 'Electrochemical Energy Storage Devices,' http://www.ima.umn.edu/2012-2013/MM8.7-16.13/abstracts.html, online, September 17, 2014.
55. J.-M. Tarascon and M. Armand, 'Issues and Challenges Facing Rechargeable Lithium Batteries,' Nature, Vol. 414, November 2001, 359 – 367.
56. Vetter, J., and et al., "Aging mechanisms in lithium-ion batteries", Journal of power sources, vol. 147, pg. 269 – 281, 2005.
57. G. Sarre, P. Blanchard, M. Broussely, 'Ageing of Lithium-Ion Batteries,' Journal of Power Sources, Vol. 127, Issues 1-2, March 2004, pp. 65-71.
58. JM. Broussely, Ph. Biensanb, F. Bonhommeb, Ph. Blanchardb, S. Herreyreb, K. Nechevc and R.J. Staniewiczc, 'Main Ageing Mechanisms in Li Ion Batteries,' Journal of Power Sources, Vol. 146, Issues 1-2, 26 August 2005, pp. 90-96.
59. M. Dubarry, B.Y. Liaw, M-S. Chen, S-S. Chyan, K-C. Han, W-T. Sie, S-H. Wu, 'Identifying battery Ageing mechanisms in large format Li ion cells,' Journal of Power Sources, In Press, Corrected Proof, Available online 17 July 2010.
60. M.M. Joglekar, N. Ramakrishnan, "Cyclic Capacity Fade Plots for aging studies of Li-ion cells," Journal of Power Sources, vol. 230, pg. 143-147, 15 May 2013.
61. John Wang, Ping Liu, Jocelyn Hicks-Garner, Elena Sherman, Souren Soukiazian, Mark Verbrugge, Harshad Tataria, James Musser, Peter Finamore, "Cycle-life model for graphite-LiFePO4 cells", Journal of Power Sources, vol. 196, iss. 8, pg. 3942-3948, 15 April 2011.
62. Karthikeyan Kumaresan, Qingzhi Guo, Premanand Ramadass, Ralph E. White, "Cycle life performance of lithium-ion pouch cells", Journal of Power Sources, vol. 158, iss. 1, pp. 679-688, 14 July 2006.
63. C. Brissot, M. Rosso, J.-N. Chazalviel, S. Lascaud, "Dendritic growth mechanisms in lithium/polymer cells," Journal of Power Sources, vol. 81–82, pp. 925-929, September 1999.
64. N. D. Williard, "Degradation Analysis and Health Monitoring of Lithium-Ion Batteries", M.S. Thesis, Dept. of Mechanical Engineering, Univ. of Maryland, College Park, MD, 2011.
65. V. Agubra and J. Fergus, "Lithium-ion Battery Anode Aging Mechanisms", Materials 2013.
66. D.A. Wetz, P.M. Novak, B. Shrestha, J.M. Heinzel, and S.T. Donahue, 'Electrochemical Energy Storage Devices in Pulsed Power,' IEEE Transactions on Plasma Science, Vol. 42, No. 10, Part 2, pp. 3034 – 3042, October, 2014.
67. D.A. Wetz, B. Shrestha, P. Novak, and Y. Chen, 'Cycling of Electrochemical Energy Storage Devices at Elevated Rates,' Journal of Directed Energy, Vol. 4, No. 4, pp. 211 – 231, Summer.
68. D.A. Wetz, B. Shrestha, and P. Novak, 'High Power Electrochemical Energy Storage for Directed Energy Applications,' SAE Int. J. Passeng. Cars – Electron. Electr. Syst., Vol.6, No. 1, May, 2013.
69. D.A. Wetz, B. Shrestha, and P. Novak, 'Elevated Rate Cycling of High Power Electrochemical Energy Storage Devices for Use as the Prime Power Source of an EM Launcher,' IEEE Transactions on Plasma Science, Vol. 41, No. 5, pp. 1319 – 1325, May, 2013.

70. P. Novak, D.A. Wetz, and B. Shrestha, 'Fast Recharge of Electrochemical Energy Storage Devices at Pulsed Elevated Rates,' IEEE Transactions on Plasma Science, Vol. 40, No. 10, Part: 1, pp. 2416 – 2424, October, 2012.
71. B. Shrestha, D.A. Wetz, and P. Novak, 'Pulsed Elevated Rate Discharge of Electrochemical Energy Storage Devices,' IEEE Transactions on Plasma Science, Vol. 40, No. 10, Part: 1, pp. 2462 – 2469, October, 2012.
72. D.A. Wetz, B. Shrestha, and P.M. Novak, 'Pulsed Evaluation of High Power Electrochemical Energy Storage Devices,' IEEE Transactions on Dielectrics and Electrical Insulation, Vol. 20, No. 4, pp. 1040 – 1048, August, 2013.
73. D.A. Wetz, B. Shrestha, P. Novak, and Y. Chen, 'Characterization of High Power Electrochemical Energy Storage Devices for use in Naval Applications,' Naval Engineers Journal, Vol. 125, No. 3, pp. 125 – 135, September 2013.
74. D. Wong, B. Shrestha, D.A. Wetz, and J.M. Heinzel, 'Impact of High Rate Discharge on the Aging of Lithium Nickel Cobalt Aluminum Oxide Batteries,' Journal of Power Sources, Vol. 280, pp. 363 – 372, April 2015.
75. D.A. Wetz, B. Shrestha, S.T. Donahue, D.N. Wong, M.J. Martin, and J.M. Heinzel, 'Capacity Fade of 26650 Lithium-Ion Phosphate Batteries Considered for use within a Pulsed Power System's Prime Power Supply,' IEEE Transactions on Plasma Science, Vol. 43, No. 5, pp. 1448 – 1455, March, 2015.
76. A. Matasso, D. Wong, D.A. Wetz, and F. Liu, 'Correlation of Bulk Internal Pressure Rise and Capacity Degradation of Commercial LiCoO2 Cells,' Journal of the Electrochemical Society (ECS), Vol. 161, No. 14, pp A2031 – A2035, 2014.
77. A.F. Matasso, D.A. Wetz, F. Liu, 'The Effects of Internal Pressure Evolution on the Aging of Commercial Li-Ion Cells,' Journal of the Electrochemical Society (ECS), Vol. 162, No. 1, pp A92 – A97, 2015.
78. A. Matasso, D. Wong, D.A. Wetz, and F. Liu, 'Effects of High-Rate Cycling on the Bulk Internal Pressure Rise and Capacity Degradation of Commercial LiCoO2 Cells,' Journal of the Electrochemical Society (ECS), Vol. 162, No. 6, pp A885 – A891, 2015.
79. D.N. Wong, A.M. Mansour, D.A. Wetz, and J.M. Heinzel, 'Degradation Behavior in Lithium Iron Phosphate Secondary Cells Under High Rate Pulsed Discharge for Complex Loads,' 228th Electrochemical Society Meeting, Phoenix, Arizona, October 11 – 15, 2015, Electrochemical Society Transactions, Pending Publication, October 2015.
80. D. Wong, B. Shrestha, D.A. Wetz, and J.M. Heinzel, 'Impact of High Rate Discharge on the Aging of Lithium Nickel Cobalt Aluminum Oxide Batteries,' Journal of Power Sources, Vol. 280, pp. 363 – 372, April 2015.
81. G. Ning, B. Haran, and B.N. Popov, 'Capacity Fade of Lithium-ion Batteries Cycled at High Discharge Rates,' J. Power Sources 2003, 117, pp. 160–169.
82. J. Lopez, M Gonzalez, J.C. Viera, and C. Blanco, "Fast-Charge Lithium-Ion Batteries for Portable Applications," 26th Annual International Telecommunications Energy Conference, Chicago, IL, September 19-23, 2004.
83. J. Li, E. Murphy, J. Winnick, P.A. Kohl, 'Studies on the Cycle Life of Commercial Lithium-ion Batteries During Rapid Charge-Discharge Cycling,' Journal of Power Sources, No 102, pp 294-301, 2001.
84. Y. Zhang and C.-Y. Wang, 'Cycle-Life Characterization of Automotive Lithium-Ion Batteries with LiNiO2 Cathode,' Journal of the Electrochemical Society, Vol. 156 (7), pp. A527-A535, 2009.

85. Q. Wang, J. Sun, and G. Chu, 'Lithium-ion Battery Fire and Explosion,' State Key Laboratory of Fire Science, University of Science and Technology of China, http://www.iafss.org/publications/fss/8/375/view, online, September 17, 2014.
86. M. Winter, Symposium on Large Lithium-ion Battery Technology and Application (AABC-06), Tutorial B, Baltimore, May 15, 2006).
87. FAA Office of Security and Hazardous Materials Safety, 'Batteries & Battery Powered Devices - Aviaion Cargo and Passenger Baggage Incidents Involving Smoke, Fire, Extreme Heat or Explosion', http://www.faa.gov/about/office_org/headquarters_offices/ash/ash_programs/hazmat/aircarrier_info/media/battery_incident_chart.pdf, online, September 19, 2014.
88. B. Jansen, 'NTSB urges more tests on Boeing 787 Dreamliner batteries,' USA Today, May 22, 2014, http://www.usatoday.com/story/news/nation/2014/05/22/ntsb-dreamliner-boeing-faa-lithium-ion-batteries-united-japan-all-nippon/9433841/, online, September 17, 2014.
89. S.J. Drake, M. Martin, D.A. Wetz, J.K. Ostanek, S.P. Miller, J.M. Heinzel, A. Jain, 'Heat Generation Rate Measurement in a Li-ion Cell at Large C-rates Through Temperature and Heat Flux Measurements,' Journal of Power Sources, Vol. 285, pp. 266-273, July 2015.
90. S. P. Miller, J. K. Ostanek, J. M. Heinzel, B. Shrestha, and D.A. Wetz, 'Temperature-Dependent Hysteresis Behavior Modeling of the Open Circuit Potential and Impedance of LiFePO4 Batteries,' Proceedings of the 17th International Meeting on Lithium-Ion Batteries (IMLB), Como, Italy, June 10 – 14, 2014.
91. K. Shah, S.J. Drake, D.A. Wetz, J.K. Ostanek, S.P. Miller, J.M. Heinzel, and A. Jain, 'An Experimentally Validated Transient Thermal Model for Cylindrical Li-ion Cells,' Journal of Power Sources, Vol. 271, pp. 262 – 268, December 2014.
92. A. Jain, D.A. Wetz, S.J. Drake, J.K. Ostanek, S.P. Miller, and J.M. Heinzel, 'Measurement of Anisotropic Thermophysical Properties of Cylindrical Li-ion Cells, Journal of Power Sources, Vol. 252, pp. 298–304, April 2014.
93. K. Shah, S.J. Drake, A. Jain, D.A. Wetz, J.K. Ostanek, S.P. Miller, J.M. Heinzel, 'Modeling of Steady-State Convective Cooling of Cylindrical Li-ion Cells,' Journal of Power Sources, Vol. 258, pp. 374-381, July 2014.
94. http://www.sigmaaldrich.com/technical-documents/articles/material-matters/electrode-materials-for-lithium-ion-batteries.html.
95. B.J. Landi, M.J. Ganter. C.D. Cress, R.A. DiLeo, and R.P. Raffaelle, 'Carbon Nanotubes for Lithium-ion Batteries, Energy Environ. Sci., 2009, No. 2, pp. 638-654.
96. http://pubs.rsc.org/en/content/articlelanding/2013/ta/c2ta01393b#!divAbstract.
97. Y. Chen, 'Lithium-Ion Technology,' Presentation delivered at UT Arlington by Saft Americas, October 2011.
98. "BU-205: Types of Lithium-ion". Battery University, Retrieved December 1, 2015, batteryuniversity.com.
99. Colthorpe, A. "German prefabricated homebuilder picks lithium iron phosphate for storage". PVTECH Storage. Retrieved on December 1, 2015, storage.pv-tech.org.
100. M. Saiful Islam and C. A. J. Fisher, 'Lithium and sodium battery cathode materials: computational insights into voltage, diffusion and nanostructural properties,' Chem. Soc. Rev., 2014, 43, 185-204
101. Chen, C.H., Liu, J., Stoll, M.E., Henriksen, G. "Aluminum-doped lithium nickel cobalt oxide electrodes for high power lithium-ion batteries", Journal of Power Sources, 128 (2) 2004, pp. 278-285.
102. http://energystorage.org/energy-storage/technologies/lithium-ion-li-ion-batteries
103. Zhang, S.S., Xu, K., Jow, T.R. "Electrochemical impedance study on the low temperature of Li-ion batteries", Electrochimica Acta, 49 (7) 2004, pp.1057-1061.

104. Song, J.Y., Wang, Y.Y., Wan, C.C. "Review of gel-type polymer electrolytes for lithium-ion batteries", Journal of Power Sources, 77 (2) 1999, pp. 183-197.
105. I.J. Cohen, J.P. Kelley, D.A. Wetz, and J. Heinzel, 'Evaluation of a Hybrid Energy Storage Module (HESM) for Pulsed Power Applications,' IEEE Transactions on Plasma Science, Vol. 42, No. 10, Part 2, pp. 2948 – 2955, October 2014.
106. I. Cohen, D.A. Wetz, J.M. Heinzel, and Q. Dong, 'Design and Characterization of an Actively Controlled Hybrid Energy Storage Module (HESM) for High Rate Directed Energy Applications,' IEEE Transactions on Plasma Science, Vol. 43, No. 5, pp. 1427 – 1433, March, 2015.
107. I. Cohen, D.A. Wetz, Q. Dong, J.M. Heinzel, and S. Veiga, 'Fuzzy Logic Control of a Hybrid Energy Storage Module for System Level Control of COTS Components Driving Pulsed Loads, Accepted for Publication in the International Journal on Fuzzy Logic Systems, November 2015.
108. I.J. Cohen, J.P. Kelley, D.A. Wetz, and J.M Heinzel, 'Impact of a Hybrid Energy Storage Module on the Power Quality of a Fossil Fuel Generator within a MicroGrid,' Proceedings of the 2014 American Society of Naval Engineers Electric Machines Technology Symposium (EMTS), Philadelphia, Pennsylvania, May 28 – 29, 2014.
109. I.J. Cohen, C.S. Westenhover, D.A. Wetz, J.M. Heinzel, and Q. Dong, 'Evaluation of an Actively Controlled Battery-Capacitor Hybrid Energy Storage Module for Use in Driving Pulsed Power Applications,' Proceedings of the 2015 IEEE International Pulsed Power Conference, Austin, Texas, May 31 – June 4, 2015, Publication Pending.
110. L. Gao, R. Dougal and S. Liu, "Active Power Sharing in Hybrid Battery/Capacitor Power Sources," in Applied Power Electronics Conference and Exposition, 2003. APEC '03. Eighteenth Annual IEEE, vol.1, pp. 497-503, Feb. 2003
111. D. Shin et al. "Battery-Supercapacitor Hybrid System for High-Rate Pulsed Load Applications," Design, Automation & Test in Europe Conference & Exhibition, 2011, pp. 1-4, March 2011
112. L. Baoquan, Z. Fang and B. Xianwen, "Control Method of the Transient Compensation Process of a Hybrid Energy Storage System Based on Battery and Ultra-capacitor in Micro-grid," in IEEE International Symposium on Industrial Electronics, pp. 1325-1329, May 2012
113. J. Dixon, I. Nakashima, E.F. Arcos, and M. Ortúzar, 'Electric Vehicle Using a Combination of Ultracapacitors and ZEBRA Battery,' IEEE Transactions on Industrial Electronics, Vol. 57, No.3, March 2010, pp. 943 – 949.
114. (http://batteryuniversity.com/learn/article/charging_lithium_ion_batteries)
115. (Q.-C. Zhuang, et al., 'Diagnosis of Electrochemical Impedance Spectroscopy in Lithium-Ion Batteries,' http://www.intechopen.com/).
116. Department of Defense Contract Award Announcements, http://www.defense.gov/contracts/contract.aspx?contractid=5339, Online, October 3, 2014.
117. Datasheets of the Deltran 480CCA, http://products.batterytender.com/Batteries/480-CCA-Lithium-Engine-Start-Battery.html.
118. Datasheets of the Saft SL2A NCA cell available either online or directly from Saft Americas. Some information presented may have come from either verbal or email conversations with Saft Americas,
119. FCvelocity®-9SSL V4 Product Manual and Integration Guide, Ballard, October 30, 2011
120. Fuel Cell, http://en.wikipedia.org/wiki/Fuel_cell, Wikimedia Foundation Inc.
121. O'Hayre, et al., Fuel Cell Fundamentals (Second Edition), © 2009, John Wiley & Sons, Hobeken, New Jersey

## LIST OF SYMBOLS, ABBREVIATIONS, AND ACRONYMS

| | |
|---|---|
| BMS | Battery Management Systems |
| BOM | Bill of Materials |
| CC | Constant Current |
| COTS | Commercial Off the Shelf |
| CV | Constant Voltage |
| DC | Diethyl Carbonate (DEC) |
| DMC | Dimethyl Carbonate |
| EC | Ethylene Carbonate |
| EIS | Electrochemical Impedance Spectroscopy |
| EMRG | Electromagnetic Railgun |
| ESR | Equivalent Series Resistance |
| HESM | Hybrid Energy Storage Modules |
| HPM | High Power Microwave |
| IED | Improvised Explosive Device |
| LCO | Lithium Cobalt Oxide |
| LFP or $LiFePO_4$ | Lithium-Iron-Phosphate |
| LIB | Lithium-Ion Battery |
| $LiNiMnCoO_2$ | Lithium-Nickel-Manganese-Cobalt Oxide |
| $LiPF_6$ | Hexafluorophosphate |
| LMO | Lithium-Manganese Oxide |
| LTO | Lithium-Titanate Oxide |
| NI | National Instruments |
| NMC | Nickel-Manganese-Cobalt |
| OCP | Open Circuit Potential |
| PC | Propylene Carbonate |
| PEM | Proton-Exchange Membrane (PEM) |
| PEMFC | Proton-Exchange Membrane Fuel Cells |
| PPEL | Pulsed Power and Energy Laboratory |
| SEI | Solid Electrolyte Interphase |
| SoC | State of Charge |
| SPICE | Simulation Program with Integrated Circuit Emphasis |
| UTA | University of Texas at Arlington |
| VI | Virtual Instrument |

DISTRIBUTION LIST

DTIC/OCP
8725 John J. Kingman Rd, Suite 0944
Ft Belvoir, VA 22060-6218 1 cy

AFRL/RVIL
Kirtland AFB, NM 87117-5776 1 cy

Official Record Copy
AFRL/RDHP/Susan Heidger 1 cy